UCRL-11978
c.2

RADIOISOTOPE CAMERAS

Hal O. Anger

March 1965

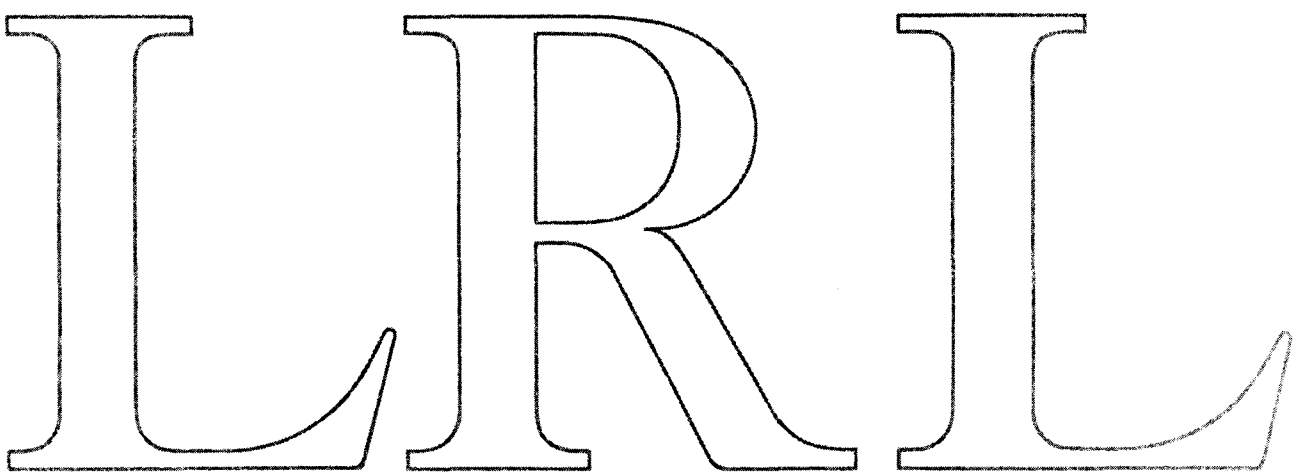

LAWRENCE RADIATION LABORATORY
UNIVERSITY of CALIFORNIA BERKELEY

UCRL-11978
c.2

DISCLAIMER

Limited distribution only

UCRL-11973

UNIVERSITY OF CALIFORNIA

Lawrence Radiation Laboratory
Berkeley, California

AEC Contract No. W-7405-eng-48

RADIOISOTOPE CAMERAS

Hal O. Anger

March 1965

Chapter 24 Outline

RADIOISOTOPE CAMERAS

Hal O. Anger

I. Nonscanning methods for translating radioisotope distribution into visual images

- A. Contact methods
- B. Camera-type devices with direct radiographic recording
- C. Scintillator mosaic with image amplifier
- D. The scintillation camera: Position-sensing multiplier-phototube array with solid sodium iodide crystal
- E. Autofluoroscope
- F. Image-converter γ-ray camera
- G. Array of γ-ray counters
- H. Spark-chamber γ-ray camera
- I. Solid-state devices

II. Detailed description of scintillation camera

- A. Principle of operation
- B. Scintillation camera with large-diameter crystal
- C. Factors affecting resolution and sensitivity
  1. Inherent detection efficiency and position resolution of sodium iodide scintillators.
  2. Accuracy of reproduction of the scintillator image on the readout oscilloscope.

I. NONSCANNING METHODS FOR TRANSLATING RADIOISOTOPE DISTRIBUTION INTO VISUAL IMAGES

Radioisotope cameras are relatively new instruments for imaging the distribution of radioisotopes in vivo. They are already useful for medical diagnosis and research, and they promise to become increasingly important in the future as more tagged compounds that localize in organs and illustrate specific functions are developed.

Modern radioisotope cameras have many advantages over radioisotope scanners. First, they take pictures much more rapidly. The speed at which they take successive pictures is limited only by the rate at which radiation information is detected, not by any mechanical factors. When a subject contains sufficient radioactivity, cameras can take pictures at the rate of one per second or faster. The speed at which scanners can take pictures is limited by how fast their probes can travel over the area.

Second, currently available radioisotope cameras gather radiation information about 10 times as fast, or in other words are about 10 times as sensitive, as conventional scanners. They achieve this sensitivity partly because they view the entire picture area continuously, while scanners view only one point at a time.

A direct result of shorter exposure times is that rapid sequences of still pictures and motion pictures can be taken to illustrate the movement of tracer compounds through organs. Scanners are inherently less suitable for this purpose because they see different parts of the subject

at different times during the scan. This can cause distorted images when the isotope distribution is changing rapidly.

Radioisotope cameras can be constructed to allow considerable flexibility in positioning patients. The patient can be sitting, standing, or lying down and the camera positioned to obtain frontal, lateral, or oblique views under any conditions. The shorter exposure times encourage taking views of organs from different angles, thus improving the visibility of lesions and other abnormalities in many cases. Also, numerical count-rate data can be obtained as a function of time for specific picture areas. For example, curves of count rate versus time can be obtained for a particular part of the kidney or a chamber of the heart.

In this chapter, the term "Radioisotope Camera" denotes any nonscanning camera-type device that images the distribution of radioisotopes. The term "γ-ray camera" refers to any type used to image single γ rays, and "positron camera" means any type that uses coincidence techniques to image positron-emitting nuclides.

The various instruments and methods used to image the distribution of radioisotopes without scanning will be briefly reviewed in this section. Then one of those instruments, the scintillation camera, is described in detail in Section II. Image-producing collimators used for γ-ray emitters are discussed in Section III, positron coincidence collimation in Section IV, and image recording methods and numerical data handling methods in Section V.

A. Contact Methods

When a radioactive subject is very thin, the simplest method of imaging the distribution of activity is to place x-ray film in contact with

the subject, expose for a length of time, and then develop the film. This is the well-known method used to obtain autoradiographs of tissue sections.

Although the contact method of imaging "sees" the whole picture area during the entire exposure time, the overall sensitivity is low because many γ rays or β particles must strike a given area on the film before visible blackening results. Therefore, exposure times are very long.

This method provides good resolution only when the distance separating the subject and film are very small. For two point sources to be resolved in the image, they should be roughly no farther from the film than they are from each other. Therefore, the contact method is not useful even for imaging the thyroid gland, which is only 2 to 3 cm below the surface. It is limited to the skin and accessible parts of the alimentary tract. Rabinowitz has reported clinical uses (47).

B. Camera-Type Devices with Direct Radiographic Recording

Of the various particles and rays emitted by radioactive isotopes, only x rays and γ rays have enough penetrating power to reach the surface of the body from deep-lying organs. Furthermore, these rays are always emitted isotropically and they can not be focused or scattered predictably. However, satisfactory images of the deeper organs of the body can be obtained by selective interference, a method of blocking out or absorbing all but a small fraction of the rays with image-producing collimators. The remaining rays travel on to form an image of the subject on the exit side of the collimator. Two such collimators are the pinhole collimator, consisting usually of a shallow hole in a conical lead shield (Section IIIA) and

the multichannel collimator, consisting of hundreds or thousands of channels in an absorber plate (Section IIIC). By either means, a γ-ray image of an object located deep within the body can be produced at a plane on the opposite side of the collimator. If a radiographic film or other detection means is located at this plane, an image of the subject can be obtained.

This method of producing images has been applied in the following ways. Roentgen in 1896 used a pinhole aperture and photographic film to obtain an image of the x-ray-emitting anode of one of his first tubes. In 1949 Copeland and Benjamin (24) used a γ-ray pinhole camera and x-ray film to obtain pictures of radium needles. In 1952 the author (2) used a γ-ray pinhole camera, a solid thallium-activated sodium-iodide intensifying screen, and blue-sensitive photographic film to obtain pictures of a metastatic thyroid lesion in vivo containing a therapeutic quantity of I^{131}. An activity concentration of 1 millicurie/cm^2 and 1 hour exposure were necessary to obtain detectable blackening of the film.

In 1953, Johansson and Skanse (38) reported the use of a multichannel collimator, solid sodium iodide crystal, and blue-sensitive film to obtain in vivo pictures of the thyroid gland and metastatic lesions. In 1955 Kellershohn and Pellerin (39) used a multichannel collimator, a mosaic of sodium iodide crystals, and mercury-vapor-sensitized film to obtain a further increase in sensitivity. In this case, each element of the crystal mosaic was lined up with a channel in the collimator. Yasukochi (58) has reported using a multichannel collimator and radiographic film to obtain images of phantom sources containing I^{125}.

However, none of the above methods of obtaining images is sensitive enough for clinical diagnostic use.

C. Scintillator Mosaic with Image Amplifier

An obvious method of improving the sensitivity of the methods described in the previous section was to convert the γ-ray image into a light image by means of a scintillator, and then amplify the light with image intensifiers. This was done in 1954 by Mortimer, Anger, and Tobias (3,46). In Fig. 1 a mosaic of 241 sodium iodide crystals, each contained in a separate cell in an aluminum holder, is shown in contact with the input of a Philips single-stage image amplifier. The tube was identical to the type intended for x-ray image amplification except the x-ray-sensitive phosphor was absent and the 5-inch photocathode was deposited directly on the inside of the glass envelope. A pinhole aperture projected a γ-ray image of the subject on the crystal mosaic. When a γ ray interacted with an element of the mosaic, light was produced, which caused electrons to be emitted from a small area of the image-amplifier photocathode. These electrons were accelerated within the tube and focused by an electron lens onto an output phosphor. The intensified image appearing at the output screen was either viewed directly or recorded on photographic film.

With this instrument, an image of a therapeutic quantity of I^{131} in the stomach of a patient with metastatic thyroid disease was observed visually. Movements of the patient's stomach were readily visible, thus indicating the value of camera-type instruments for dynamic studies. However, the sensitivity was still too low for diagnostic use. Because of field emission in the image amplifier, the background was equivalent to

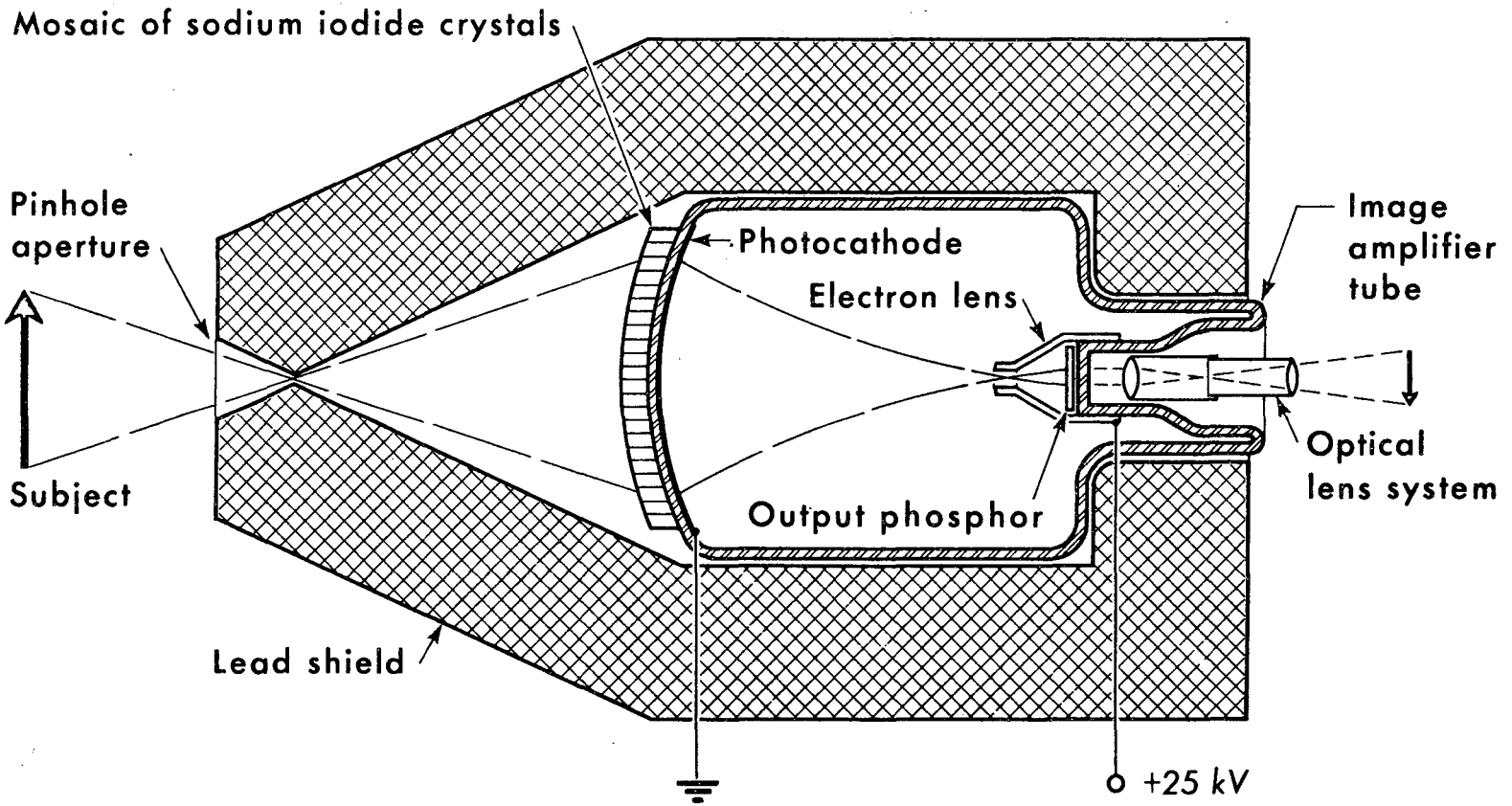

Fig. 1. Early gamma-ray camera employing mosaic of sodium iodide crystals and image amplifier (46).

10 $\mu C/cm^2$ when photographic recording was used, and because of the low gain of the image amplifier, an activity concentration of 200 μ/cm^2 of I^{131} was necessary for visual observation. Despite the low sensitivity, this instrument clearly demonstrated the potential usefulness of camera-type imaging devices.

D. The Scintillation Camera: Position-Sensing Multiplier-Phototube Array with Solid Sodium Iodide Crystal

A new approach to a sensitive camera-type instrument was taken by the author in 1956 (4,5). The result is the scintillation camera, which employs a solid sodium iodide scintillation crystal viewed by an array of multiplier phototubes, as shown in Fig. 2. A computing circuit, used in combination with the phototube array, senses the position of scintillations in the crystal and sends signals to an image-readout oscilloscope that reproduces the scintillations as point flashes of light. A time exposure of the oscilloscope screen is taken with a Polaroid camera, and an image of the active areas of the subject results. Pinhole and multichannel collimators are used to image γ-ray emitters, and coincidence collimation of annihilation radiation is used for positron emitters.

The signals from the phototubes are summed and pulse-height selection is employed to eliminate scintillations not falling within the photopeak of the γ-ray spectrum, thus reducing background by the same method as used in conventional radioisotope scanners. Excellent pulse-height resolution results from the efficient collection of light from the sodium iodide crystal.

By the use of a solid homogeneous scintillator rather than a mosaic, the images have no distracting patterns superimposed. When a scintillation

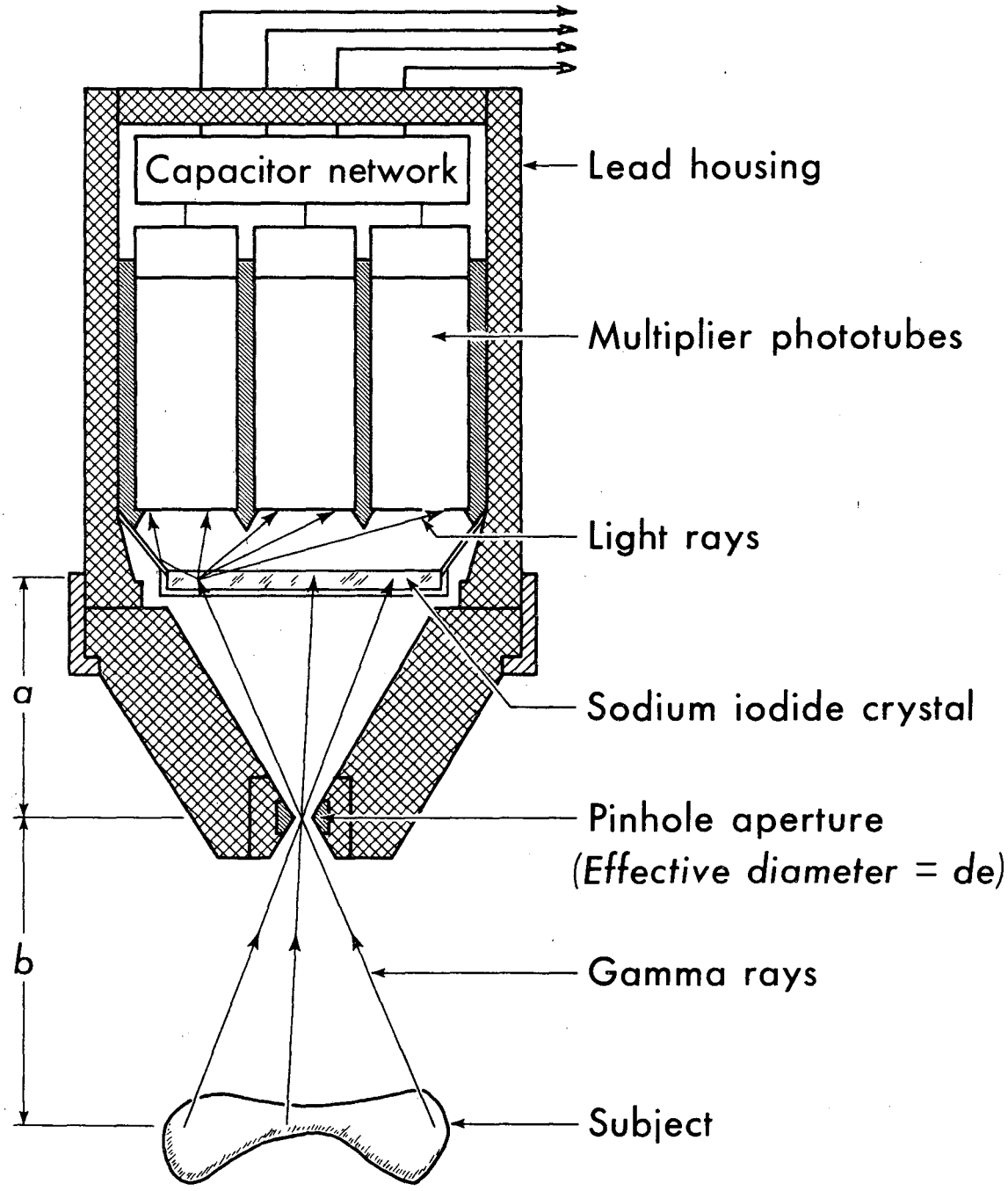

Fig. 2. Early scintillation camera with 4-inch-diameter solid sodium iodide crystal and seven multiplier phototubes (4, 5).

occurs at an intermediate point between phototubes, its position is still accurately determined because of the proportionate division of light among the tubes. The accuracy of determining the position of scintillations in recent cameras allows about 1000 picture elements to be resolved in the crystal at medium γ-ray energies.

By the use of the phototube array, many of the limitations of image amplifiers are avoided. High gain is readily obtained, tube background is negligible, and there is convenient remote reproduction of the images. Coincidence and dot-shifting techniques are easily used in conjunction with positron emitters, as discussed in Section IV. Also, there is no practical limit to the size of the camera except for limitations in the manufacture of the sodium iodide crystal. Early models used crystals as small as 4 inches in diameter. Recent models, including one that is commercially available,* employ 11-inch-diameter crystals viewed by an array of 19 multiplier phototubes (8, 9). Still larger cameras will be built in the future.

The useful γ-ray-energy range of scintillation cameras is about 0.07 to 0.7 MeV. The upper limit is set by the inherent difficulties of collimating and detecting high-energy γ rays. The lower limit is a result of statistical phenomena discussed in Section II C2.

With the 11-inch cameras, pictures of nearly all organs of the body can be taken in about 1/10 the time required by conventional radioisotope scanners. Brain tumor pictures have been taken in 10 seconds, and stop-motion pictures have been taken of isotopes going through the heart at the rate of one picture per second (14).

---

*Nuclear-Chicago Corporation, 333 Howard Avenue, Des Plaines, Illinois.

The design and performance of a scintillation camera employing a 4-3/4-inch-diameter sodium iodide crystal, 7 phototubes, and a direct-view storage cathode-ray tube have been described by Mallard and Myers (43). The storage tube used for display of the image allows each scintillation to be shown as a persistent point of light, rather than a momentary flash. As more dots appear and merge into each other, a half-tone picture of the subject builds up on the screen. This can be observed as it occurs, and the exposure can be stopped when a satisfactory picture is obtained. Furthermore, the brightness and background cutoff level can easily be varied to suit the particular subject. The screen is photographed at any time to obtain a permanent record.

Additional information on scintillation cameras is given in Section II.

E. Autofluoroscope

In 1962, Bender and Blau (16, 17) reported construction of a γ-ray imaging instrument called the autofluoroscope. It employed a mosaic of 297 sodium iodide crystals, each 3/8 inch in diameter by 2 inches long, viewed by a position-sensing multiplier phototube array. The electronic circuit and image readout system was the same as that employed for the scintillation camera and described in Section II A1. Collimation was achieved with a multichannel collimator having 297 tapered holes, one corresponding to each mosaic element. Television contrast enhancement was used in the display of the final image (18).

The purpose of the thick mosaic scintillator was to obtain high detection efficiency for medium- and high-energy γ rays. While this was doubtless obtained, the sensitivity of radioisotope cameras depends as much on the efficiency of the collimator as on the efficiency of the scintillator.

Calculations indicate the collimator used with the autofluoroscope was relatively inefficient compared to other multichannel collimators. The net sensitivity, in terms of the number of γ rays detected per minute per microcurie of activity in the subject, was not reported.

With this instrument pictures of brain tumors and liver tumors were made with 1/5 to 1/10 the exposure times usually required with a conventional scanner. Also dynamic studies were made of I^{131} hippuran going through a kidney and Ba^{137m} going through the heat (18).

Except for the above examples, very few pictures taken with this instrument have been published, and no comprehensive comparative studies have been reported.

The same authors have recently described a new rank-and-file coincidence method for determining which crystal in a mosaic detects a γ ray, and a system of recording the counts from each mosaic element in digital form in a magnetic core memory system (18, 19).

F. Image-Converter γ-Ray Camera

In 1963 Ter-Pogossian et al. (51) reported the instrument shown in Fig. 3 which was designed for use with low-energy γ-ray emitters. It employed an 8-inch-diameter image-amplifier tube originally designed for use as an x-ray image intensifier. This type of tube has a thin x-ray-sensitive phosphor inside a glass envelope. When an x ray interacts with the phosphor, light is emitted which in turn causes electrons to be emitted from a photocathode deposited on the phosphor. These electrons are accelerated and focused by an electron lens onto an output screen. Each x ray that interacts with the input phosphor produces several thousand

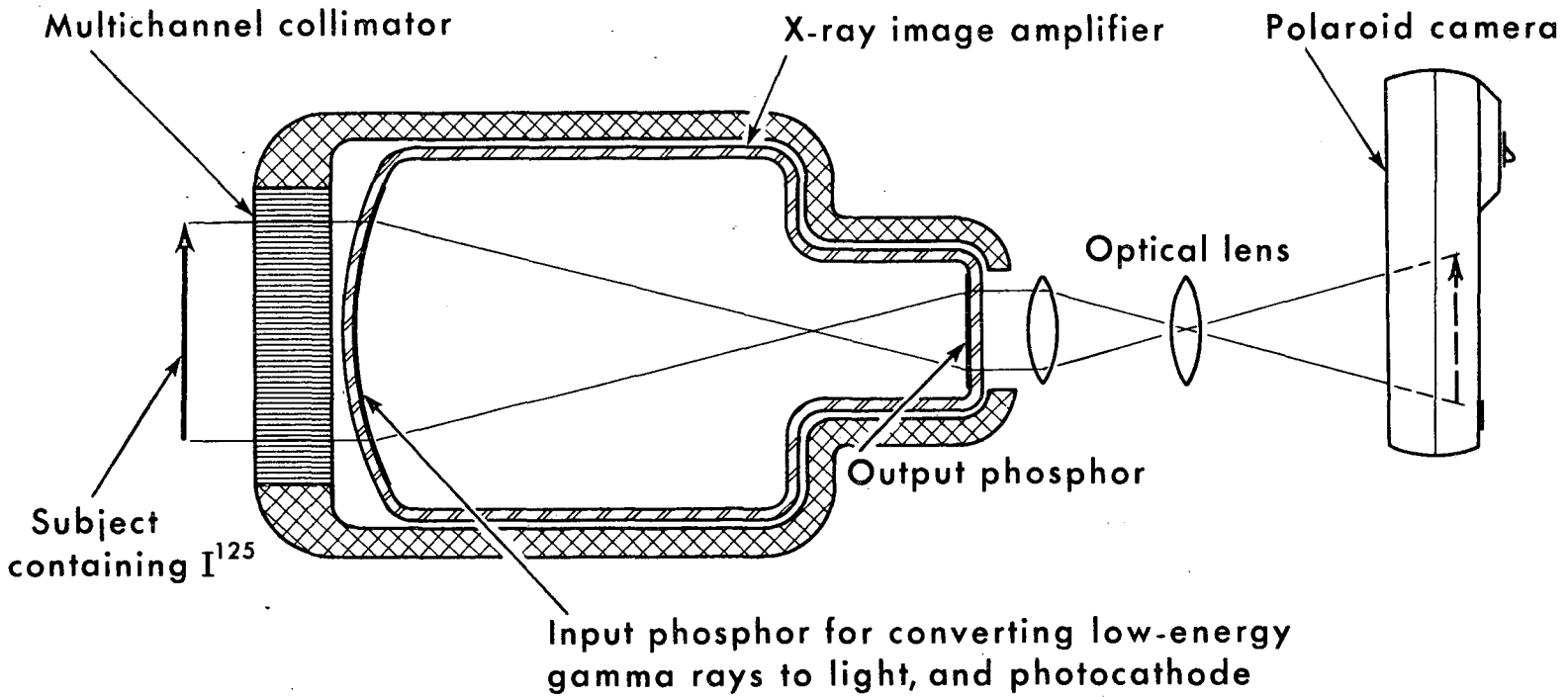

MUB-5594

Fig. 3. Gamma-ray camera employing x-ray image amplifier. This camera is for use with low-energy γ-ray emitters such as I^{125} (51).

light photons at the output screen. The amplified flashes appearing at the output are recorded on fast Polaroid film.

This instrument was first used with the 27-keV x rays from I^{125}. A multichannel collimator was employed to project an image of the subject on the input phosphor. Approximately 26% of the x rays that impinged on the glass envelope interacted with the input phosphor and produced a visible dot in the image. Pictures of phantoms containing as little as 25 μC of I^{125} were taken in 3 minutes. However, the first instrument was not applied clinically, because in its existing form, the large diameter of the image amplifier did not allow getting the instrument close enough to the thyroid gland of a patient. Also the input phosphor was located an appreciable distance inside the glass envelope of the image amplifier tube, thus reducing the resolution of the x-ray image obtained from the multichannel collimator.

With specially constructed image-intensifier tubes, this type of instrument should provide good results with low-energy emitters. It has the advantages of simplicity and good detection efficiency for x rays and low-energy γ rays, and it promises good resolution when modified image amplifier tubes are available.

Its disadvantages include low detection efficiency for medium-energy γ rays, and a lack of pulse-height selection to reduce background from scattered rays. Furthermore, x-ray emitters and low-energy γ-ray emitters have inherent disadvantages for imaging deep-lying organs. More Compton scattering occurs in tissue at these energies and fewer of the scattered rays can be removed by pulse-height selection even if it is

provided (49) (see Section II D2). The net effect is a higher background of scattered dots in the images.

A similar instrument was reported by Kellershohn and Pellerin (40) in 1955. However, low-energy γ-ray emitters were not in use at that time and image amplifiers had higher backgrounds, so satisfactory sensitivity for clinical purposes was not obtained.

G. Array of γ-Ray Counters

In 1955, Fucks and Knipping (27) reported constructing an instrument called the Gamma-Retina. It employed a fixed array of 39 Geiger-Müller counters and a collimator consisting of a lead plate with 39 holes, one corresponding to each counter. Whenever a γ ray was detected by a counter, a flash appeared in an array of glow lamps at a point corresponding to the position of the counter in the array. The flashes were photographed with a motion picture camera to record the movement of tracer compounds. In 1964, an improved model was described that employed 100 scintillation counters in a 17×17-cm array (28). An intensity-modulated cathode-ray oscilloscope was used to display the detected γ rays. This instrument was built primarily to study heart function and to detect heart shunts in vivo by means of isotope angiocardiography. For preliminary studies with large dogs, 50 mC of 7-day Lu^{177} were injected and pictures were taken at a rate that showed the isotope traveling through the chambers of the heart.

Gross et al. (35) in 1964 reported construction of a similar instrument built primarily for kinetic studies of tracer compounds in the brain. This instrument employed two 6×8-inch arrays of 63 scintillation

counters each. A small focused collimator was provided for each counter. The counts from each counter were stored in a magnetic-core memory system. Numerical readout was by means of punched tape or typewriter, and images with any degree of background erase could be displayed on an oscilloscope.

Although simple in concept, these instruments are complex in construction and maintenance, and their resolution is limited to the center-to-center distance between counters in the array.

H. Spark-Chamber γ-Ray Camera

In 1964, Kellershohn et al. (41) reported development of a new and very simple low-energy γ-ray camera employing a spark chamber as the image detector. The 8-inch-diameter chamber is filled with argon or xenon gas, and a potential of several kilovolts is maintained between a disc-shaped cathode and two grids. When x rays or γ rays produce recoil electrons in the gas between cathode and first grid, the potential difference causes additional free electrons and ions to be produced by collisions until an avalanche follows. The charged particles travel to the second part of the chamber, where they form the path for a visible spark. The sparks are photographed through a glass end of the chamber by an optical camera.

At the time of reporting, the detection efficiency of the spark chamber for the ≈ 30 keV x rays from I^{125} was 1%. Kellershohn states that higher efficiencies can probably be obtained in the near future.

I. Solid-State Devices

A new method of detecting γ rays has been under development during the past few years, namely by means of solid-state semiconductor detectors (Chapter). A mosaic of such detectors connected to a suitable

image readout device and used with conventional pinhole or multichannel collimators offers an alternative method of producing a γ-ray camera.

At present the gross detection efficiency of the largest available germanium solid-state detectors is limited to about 30% for 0.3-MeV γ rays, and the photopeak detection efficiency is about 5% for the same γ rays (50). The low detection efficiency compared with sodium iodide scintillators results because they are made from low-atomic-number material, and their sensitive volume is less than 1 cm thick.

Solid-state detectors offer the potential advantage of much better pulse-height resolution than scintillation detectors, and thus more scattered γ rays could be rejected if these detectors could be employed. Mosaics with 100 or more elements are presently very expensive. Also, for best pulse-height resolution they must be operated at liquid nitrogen temperatures. Practical cameras using these detectors have yet to be developed.

II. DETAILED DESCRIPTION OF SCINTILLATION CAMERA

A. Principle of Operation

The principle of operation of the phototube-array scintillation camera is illustrated in the drawing of the early model shown in Fig. 2. It employed a 4-inch-diameter by 1/4-inch-thick sodium iodide crystal viewed by seven 1.5-inch-diameter multiplier phototubes. The phototubes were arranged in a hexagonal array with six of the tubes at the points of a hexagon and the seventh at the center. The central plane of the crystal was about 1 inch from the photocathodes, thus allowing light from each scintillation to divide among the tubes.

The circuit for computing the location of scintillations and displaying them on the image-readout oscilloscope is shown in Fig. 4. Pulse signals from the phototubes are fed through small capacitors to four output leads called the X^+, X^-, Y^+, and Y^- leads. The amount of signal transferred to each output lead is proportional to the capacitance value in picofarads given in the diagram. For instance, phototube No. 1 has a 30-pf capacitance to the X^+ lead, 10 pf to the X^- lead, 40 pf to the Y^+ lead, and zero capacitance to the Y^- lead. Therefore this phototube transfers most of its signal to the X^+ and Y^+ leads. Tube No. 7 in the center of the array has 20 pf to each lead, and therefore sends equal signals to the four leads.

Suppose a scintillation occurs directly under phototube No. 2. The light is emitted isotropically. Most of it is collected by phototube No. 2 because this tube is closest and subtends a large solid angle. Smaller

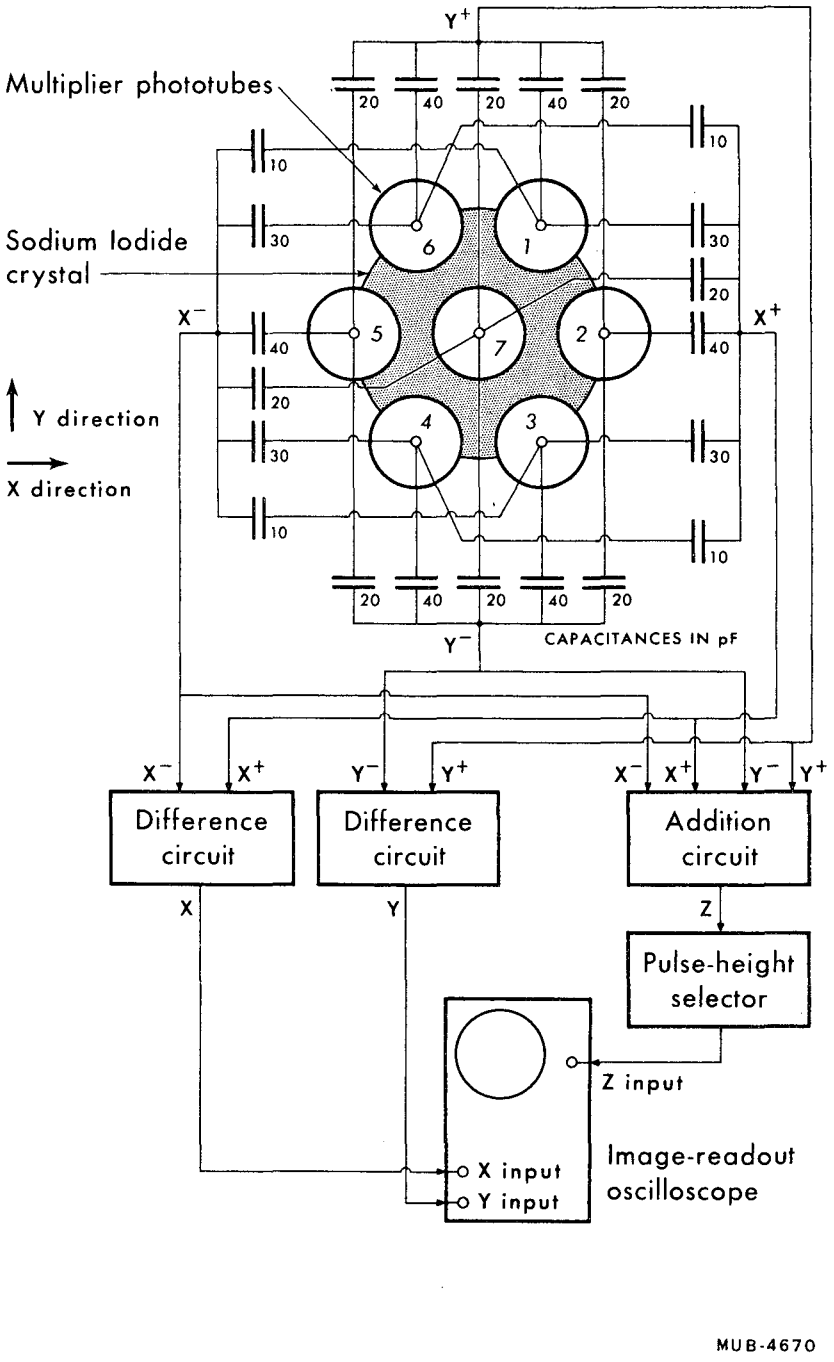

Fig. 4. Block diagram showing principle of operation of scintillation camera.

amounts are collected by tubes Nos. 1, 3, and 7, and still smaller amounts by tubes Nos. 4, 5, and 6. A large X^+ signal is generated by this scintillation because tube No. 2 is connected by a large capacitance to the X^+ lead. A small X^- signal is generated, and moderate but equal Y^+ and Y^- signals are generated.

These four signals are applied to analog computer elements and three new signals reproduced that indicate the position and brightness of the scintillation. Signals approximately proportional to the X and Y coordinates of the scintillation are obtained as follows:

$$X = X^+ - X^-,$$
$$Y = Y^+ - Y^-.$$

The origin of the coordinate system is located at the center of the crystal. These equations assume that all scintillations are of equal brightness. For reasons given below the only scintillations displayed on the readout oscilloscope are equal in brightness (i.e., photopeak scintillations) so the above condition is met. The X and Y signals are applied directly to the X and Y inputs of the image-readout oscilloscope.

A third signal which is proportional only to the brightness of the scintillation without regard to its location in the crystal is called the Z signal. It is obtained as follows:

$$Z = X^+ + X^- + Y^+ + Y^-.$$

This signal is applied to the input of a single-channel pulse-height selector. The window of the pulse-height selector is adjusted to accept only the photopeak of the γ-ray spectrum. Most scattered γ rays and many due to natural background are eliminated because they do not meet the pulse-height requirement.

To return to the description of what happens when a scintillation occurs under tube No. 2: when the X^+, X^-, Y^+, and Y^- signals are applied to the difference circuits, the X circuit puts out a large positive signal because the amplitude of the X^+ signal is large, and the Y circuit puts out a signal of zero amplitude because the Y^+ and Y^- signals are equal.

Normally, the beam of the image-readout oscilloscope is directed to the center of the screen and is cut off by a negative voltage on the control grid of the cathode-ray tube. When the X and Y signals are applied, the beam is deflected to a point on the right-hand side of the screen for a period of 1 microsecond. At the same time, the X^+, X^-, Y^+, and Y^- signals have been summed in the addition circuit and the resulting Z signal applied to the input of the pulse-height selector. If the Z signal has the prescribed amplitude, the pulse-height selector produces an output pulse that turns on the beam of the image-readout oscilloscope for 0.5 microsecond. The scintillation is reproduced as a point flash of light on the right-hand side of the oscilloscope screen.

Therefore, the cathode-ray tube presents a continuous readout of photopeak scintillations occurring in the crystal. The flashes are photographed over a period of time with an optical scope camera, and the resulting picture shows the distribution of activity in the subject. Exposure times last from a second to a few minutes or more, and usually 1,000 to 100,000 or more dots are recorded on each picture.

Although only seven phototubes are used in this model of the scintillation camera, hundreds of picture elements can be resolved, because the scintillations are reproduced in approximately correct locations even when

they occur at points intermediate between the phototubes. How accurately the position of the flashes on the readout oscilloscope corresponds to the original scintillations can easily be demonstrated by test pictures. Examples are shown for a larger instrument in Section IIC.

In the early scintillation cameras, a pinhole collimator was usually used to project a γ-ray image of the subject onto the crystal. Apertures from 1/8 to 5/16 inch in diameter were employed. In clinical practice these small instruments were used mostly for visualization of the human thyroid gland with I^{131}.

They were also used to show the distribution of γ-ray-emitting isotopes in small animals. The first "isotope motion pictures" showing the movement of a tracer compound in vivo were taken in 1958. A series of still pictures from this film is shown in Fig. 5. They show 50 μC of I^{131} Rose Bengal being taken up by the liver and excreted into the duodenum of a rat. Pictures were taken at the rate of one frame per minute.

B. Scintillation Camera with Large-Diameter Crystal

With the availability of large sodium-iodide crystals, large scintillation cameras were constructed (8, 9, 14). The thicker crystal and an increased number of phototubes yield instruments with higher sensitivity and improved overall resolution. An outline drawing of the γ-ray-detecting head of a camera employing an 11.5-inch-diameter crystal is shown in Fig. 6. The scintillator is viewed by a hexagonal array of nineteen 3-inch-diameter multiplier phototubes. The phototubes are spaced about 1.5 inches from the central plane of the scintillator and are optically coupled to the phototubes by means of a Lucite light pipe or a mineral-oil

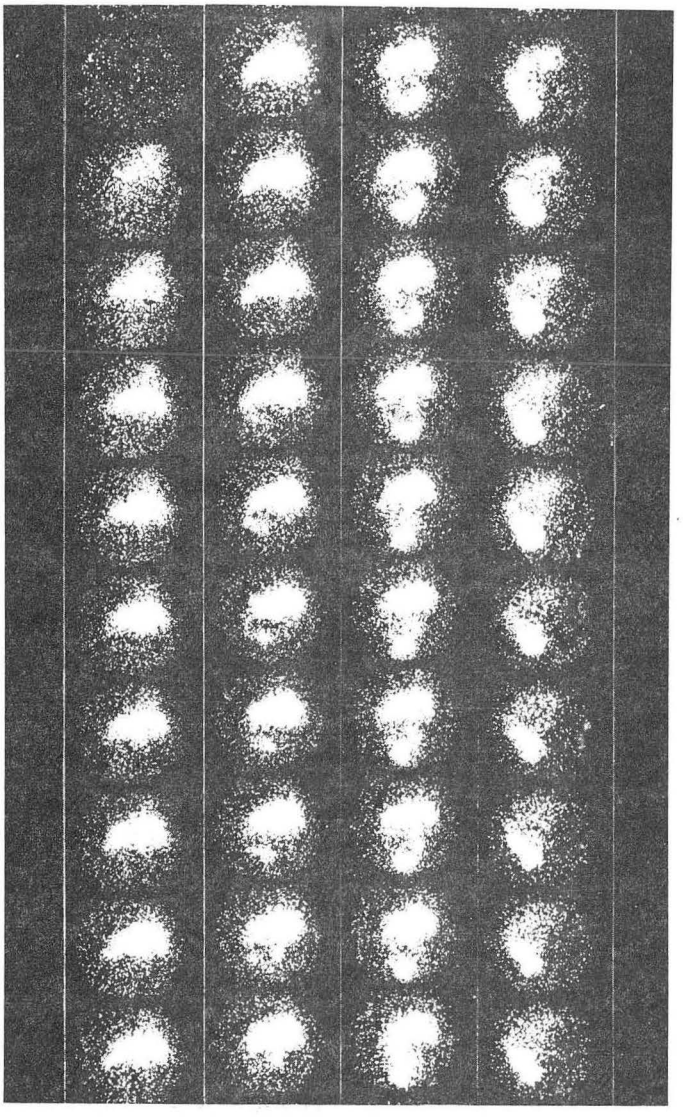

ZN-4774

Fig. 5. "Isotope movies" showing 50 μC of I^{131} rose bengal taken up and excreted from liver of rat. Pictures were taken at 1 frame per minute. Scintillation camera and pinhole collimation were used.

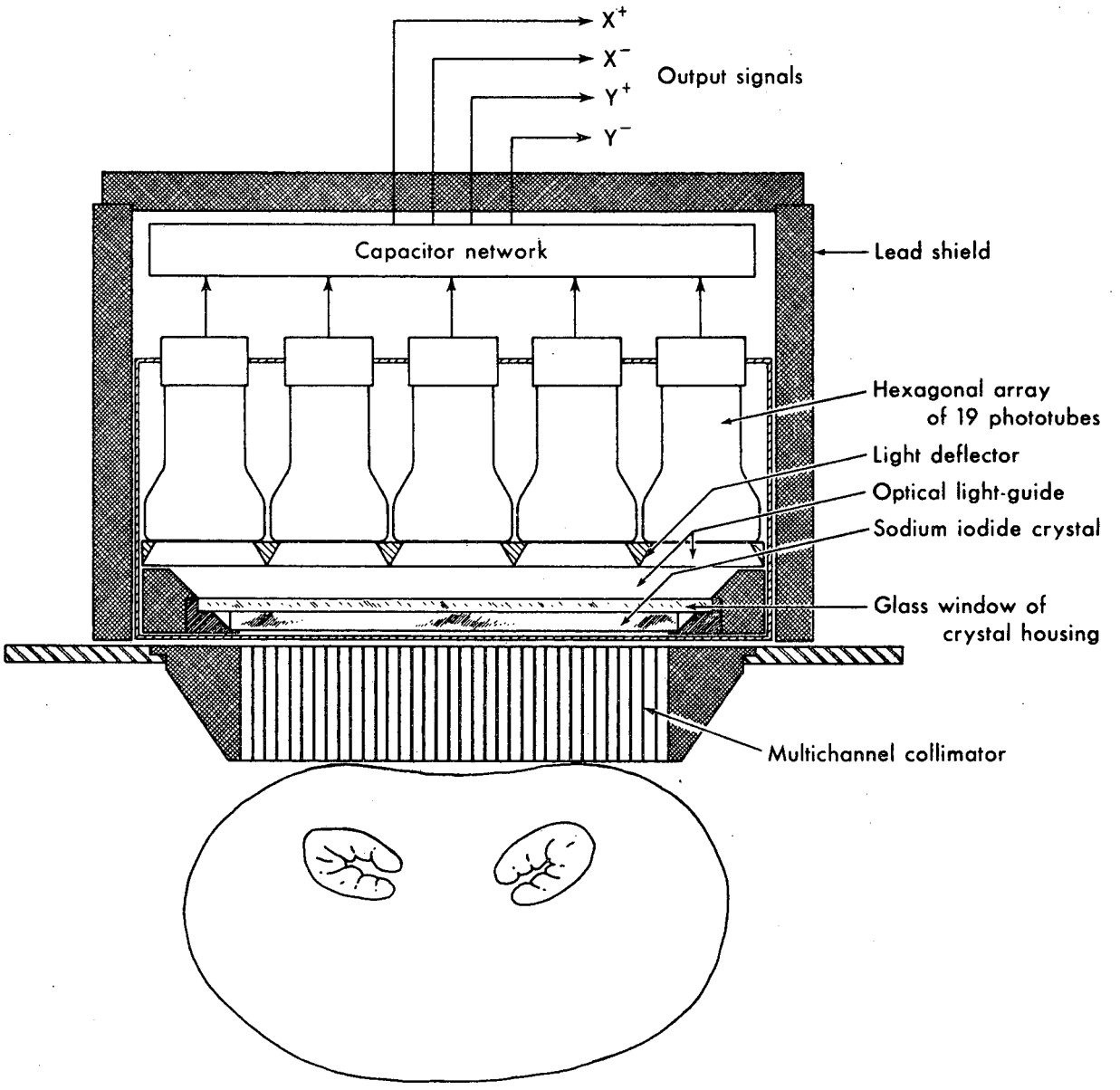

Fig. 6. Image detector of scintillation camera employing 11.5-inch-diameter by 0.5-inch-thick solid sodium iodide crystal and 19 multiplier phototubes. Multichannel collimator is shown.

bath to maintain a high-refractive-index path between the crystal and the phototubes. The crystal is rough on all sides to reduce piping of the light to the edges of the crystal by repeated internal reflection. It is contained in a hermetically sealed can with a glass window and aluminum oxide reflector. A light deflector adjacent to the phototubes, shown in cross section in Fig. 6, reflects light that would normally fall between the tubes. This important component has been found empirically to improve the resolution and linearity of the pictures. The combination of elements including the scintillator crystal, multiplier-phototube array, optical coupler, and the capacitor network is called an image detector.

A block diagram of the electronic circuit is shown in Fig. 7. The extra components used for coincidence collimation of annihilation radiation from positron emitters are also shown. The basic principle of operation of this large camera is the same as for the small camera described in Section IIA. The capacitor network is more complicated because of the larger number of phototubes employed. Details are given in another publication (9).

Recently the difference circuits have been replaced with ratio circuits that perform the function

$$X = \frac{X^+ - X^-}{Z} \quad \text{and} \quad Y = \frac{Y^+ - Y^-}{Z} .$$

With these circuits, the positions of flashes on the image-readout oscilloscope are independent of the brightness of the scintillation. Therefore, wide pulse-height-selector windows can be used without the slight loss of position resolution that occurred at the edges of the pictures when difference circuits were used.

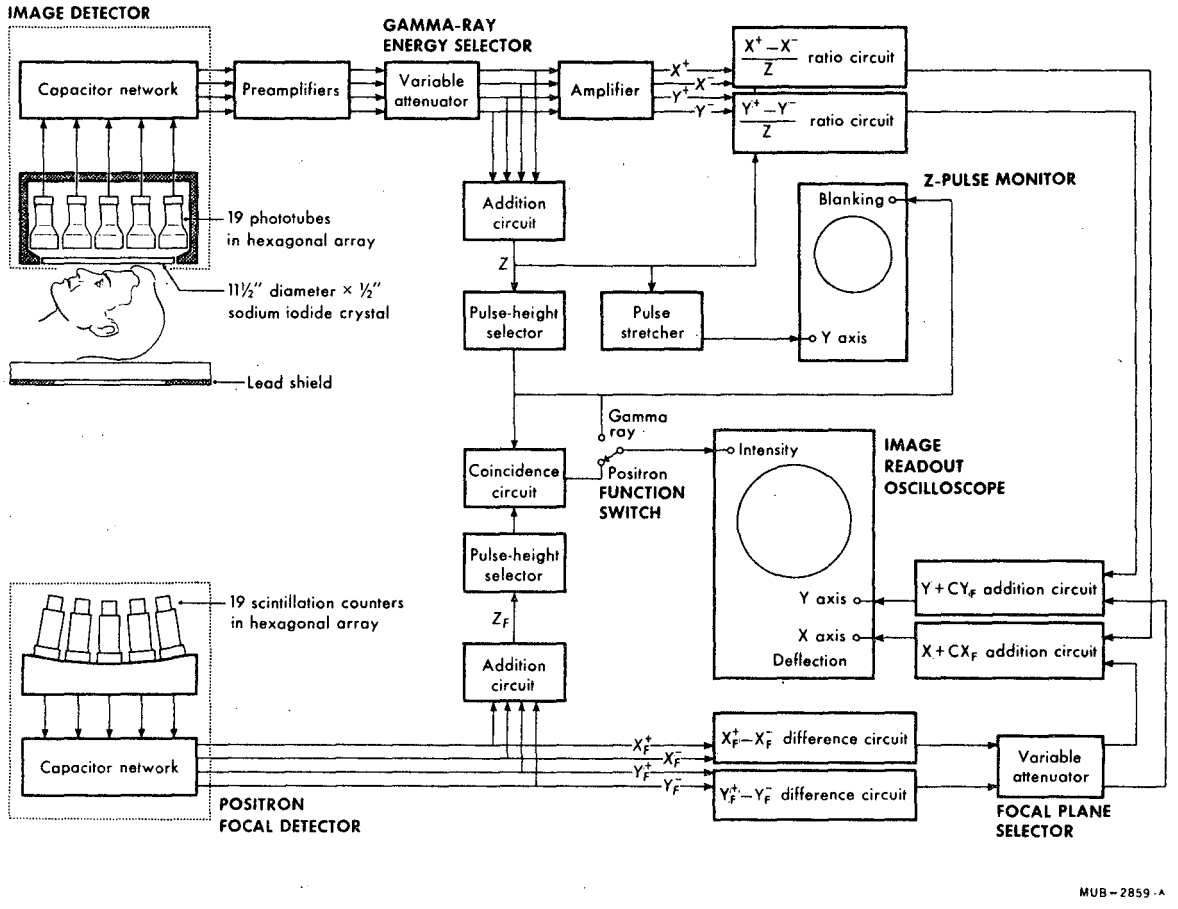

Fig. 7. Block diagram of γ-ray and positron scintillation camera employing image detector shown in Fig. 6.

The γ-ray-energy selector shown at the top of Fig. 7 is a variable attenuator that permits setting the scintillation camera to an isotope of given γ-ray energy while the voltages on the phototubes are kept constant. The method of adjusting the phototube voltages so that all have equal gain is described in another publication (9). It is easily accomplished with a collimated γ-ray source and the Z-pulse monitor oscilloscope described in the next paragraphs.

The Z-pulse monitor oscilloscope, shown at upper right of Fig. 7, gives the operator a means of quickly adjusting the pulse-height-selector window to the photopeak of the isotope being used. The width of both the window and the photopeak, and their relation to each other, can be observed visually. In this type of display, the width of the photopeak is represented by the vertical width of the bright line shown in Fig. 8A. The window is represented by the small superimposed dark area shown in Fig. 8B. The vertical width of the dark area is proportional to the width of the window. A properly adjusted window is shown in Fig. 8C. This type of display is especially valuable when double isotope studies are performed, because the two photopeaks produce two bright lines and the window can be adjusted to coincide with either one of them very quickly. Unsymmetrical adjustments can also be easily made when necessary in double isotope studies, or in cases where it is desirable to reduce acceptance of scattered γ rays to a minimum (49).

The pulse-height resolution obtained with the image detector described here is equal to that of a good scintillation counter. This is due to the efficient light collection from the solid crystal and the direct coupling to the phototubes. The full width of the photopeak at half maximum is

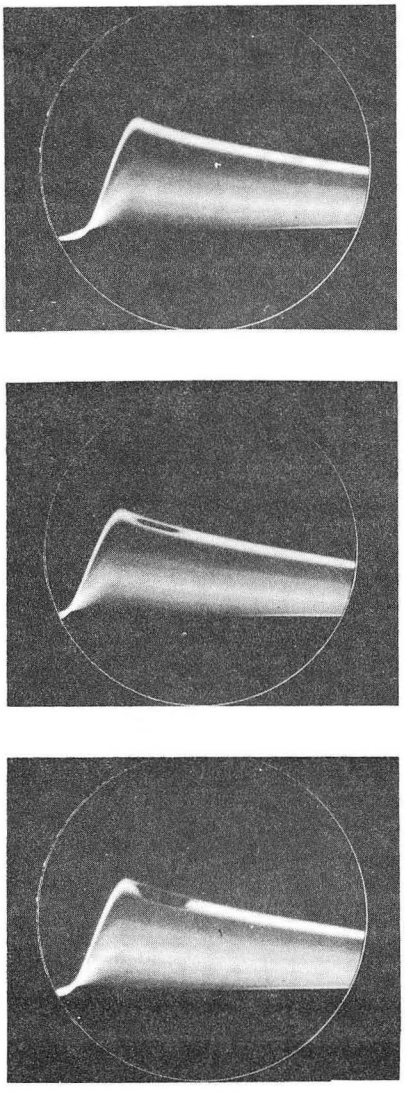

Fig. 8. Display seen in Z-pulse monitor scope. (A) Narrow white line at top is photopeak of Ga^{68}. (B) Window of pulse-height selector is centered on photopeak line but window is too narrow to accept full photopeak. (C) Window width and height in proper adjustment.

typically 8.7% for Cs^{137} and 13.8% for Hg^{203} when the entire scintillator is irradiated with γ rays. Good pulse-height resolution has the important advantage that a narrow pulse-height-selector window can be used, providing maximum rejection of γ rays scattered by the subject and collimator. Maximum reduction of background due to cosmic rays and stray radioactivity is also obtained.

C. Factors Affecting Resolution and Sensitivity

The overall sensitivity of the scintillation camera is determined by two factors, namely the geometric efficiency of the collimator and the photopeak detection efficiency of the scintillator. The former is defined as the fraction of γ rays emitted from the subject that pass through the collimator, and the latter is defined as the fraction of γ rays impinging on the crystal that produce photopeak scintillations. Both factors are subject to approximate mathematical analysis.

The overall resolution is determined by three factors, the inherent resolution of the γ-ray image produced by collimators, the translation of this γ-ray image into a light image by the scintillator, and the accuracy of reproduction of the image in the scintillator on the image-readout oscilloscope.

The resolution and efficiency of γ-ray collimators is considered mathematically in Section III. The resolution and efficiency of positron coincidence collimation is considered in Section IV. The inherent position resolution obtainable from solid sodium iodide crystals, and the accuracy of reproduction of the image on the readout oscilloscope, are considered in the remainder of this section. In other types of imaging systems, additional factors may be important, such as the resolution of image amplifiers, the size of mosaic elements, etc., but these factors

are not relevant here.

1. Inherent Detection Efficiency and Position Resolution of Sodium Iodide Scintillators

In the normal operation of the scintillation camera, each photopeak event that occurs in the image detector crystal is recorded as a visible dot on the picture. Photopeak events can result either from simple photoelectric interactions between the γ ray and the crystal or from multiple Compton-photoelectric interactions. The resolution of the image is decreased by the multiple interactions for reasons outlined below. Monte Carlo calculations have been performed to determine the image-resolution loss and the theoretical photopeak detection efficiency in sodium iodide as a function of γ-ray energy and scintillator thickness (10). Before the results of the calculation are presented, a detailed description is given of the types of interactions that occur.

Primary photoelectric interactions. In this kind of event, the original γ ray disappears and a photoelectron absorbs all of its energy. Light is emitted along the path of the electron, but its path length is very short. For instance, the range of a 0.36-MeV photoelectron in sodium iodide is 0.25 mm (48). In the image-resolution calculations all the light is assumed to come from the point where the interaction occurred. At low γ-ray energies, primary photoelectric interactions are the main contributors to the photopeak in sodium iodide.

One or more Compton interactions followed by escape of a secondary γ ray from the scintillator. In this kind of event, part of the energy of the original γ ray is transferred to a Compton electron, and the remaining energy is carried away by a secondary γ ray. If the secondary γ ray

escapes the scintillator, the interaction does not contribute to the photopeak of the pulse-height spectrum, because the Compton electron produces a relatively weak scintillation. The effect of these events on the photopeak detection efficiency and image resolution is not considered in the calculations because it was assumed they are rejected by the pulse-height selector.

One or more Compton interactions within the scintillator followed by photoelectric interaction of a secondary photon. These events contribute to the photopeak, since all the energy of the orginal γ ray is absorbed in the scintillator. The scintillation from the first Compton electron is correctly positioned on the path of the primary γ ray, but the secondary scintillations are located a distance away. The computing circuit of the scintillation camera places a single flash on the oscilloscope at a point corresponding to the center of luminous intensity of the scintillations. The probability of this kind of event as a function of the perpendicular distance from the primary γ ray to the center of intensity was calculated. These multiple Compton-photoelectric events are the main contributors to the photopeak at the higher γ-ray energies.

The gross detection efficiencies as a function of γ-ray energy for 1/8-inch- to 2-inch-thick crystals of sodium iodide, as determined by analytic calculation, are shown in Fig. 9. The gross detection efficiency is the probability of producing a scintillation of any kind, either Compton or photoelectric. The photopeak detection efficiency for the same crystals, as determined by the Monte Carlo calculation, are shown in Fig. 10. For a 1/2-inch-thick crystal, typical photopeak detection efficiencies are 90% for 0.15-MeV, 44% for 0.28-MeV, 29% for 0.36-MeV, and 17% for 0.51-MeV γ rays.

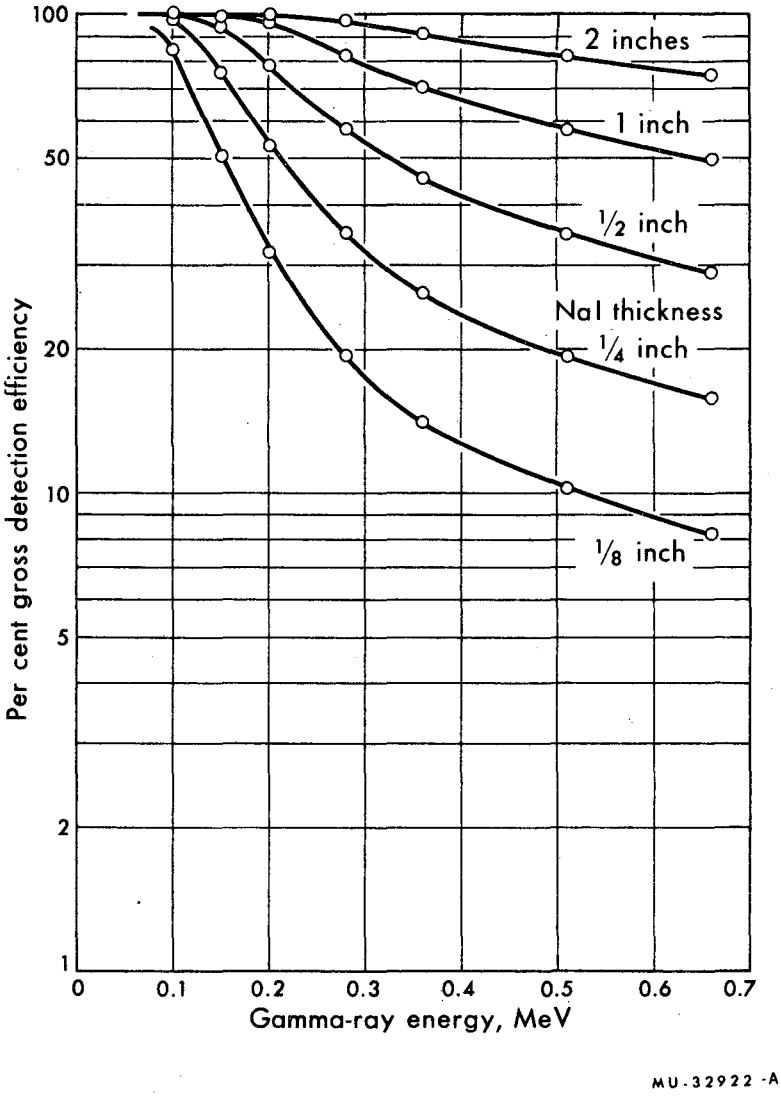

Fig. 9. Calculated gross (Compton + photoelectric) detection efficiency for sodium iodide as a function of γ-ray energy and crystal thickness. Gross detection efficiency is defined as the fraction of γ rays striking the crystal that produce either Compton or photoelectric scintillations (10).

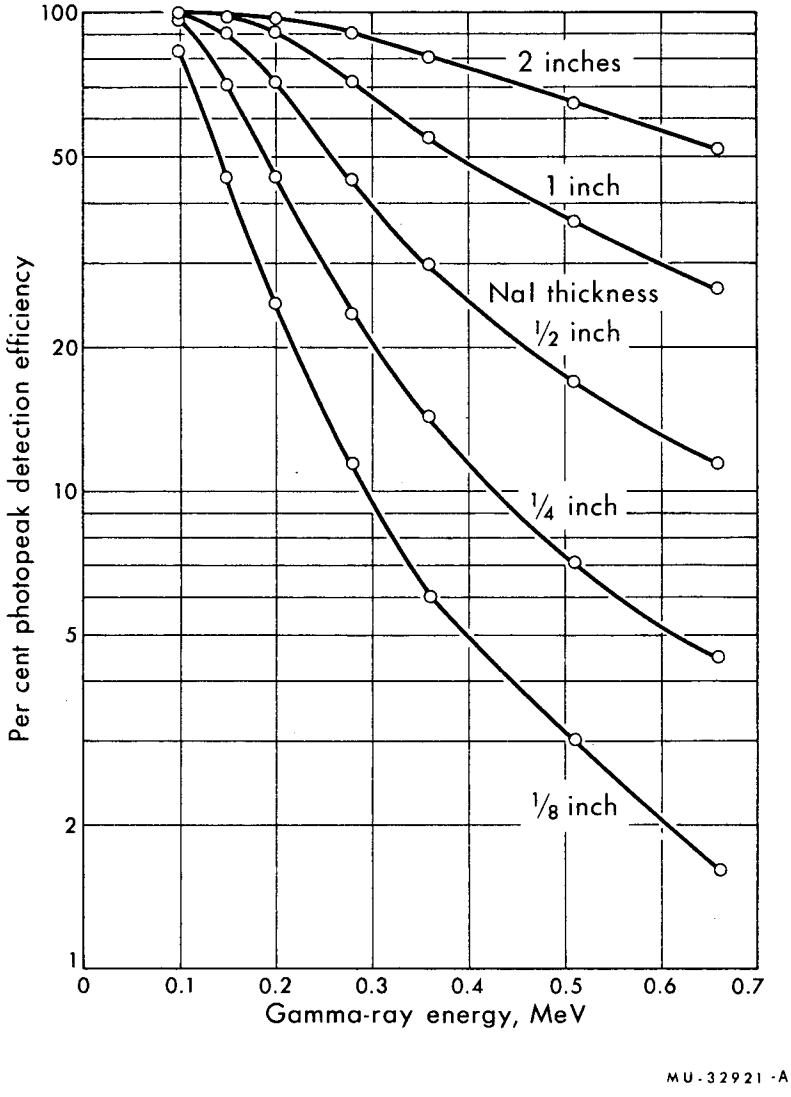

Fig. 10. Calculated photopeak detection efficiency for sodium iodide. Photopeak detection efficiency is defined as the fraction of γ rays striking the crystal that produce either a direct photoelectric interaction or a multiple Compton-photoelectric interaction (10).

The theoretical loss of image resolution due to multiple Compton-photoelectric events in the scintillator is shown in Fig. 11. The numbers of primary photoelectric events are shown in the shaded columns, and the remaining portions of the curves show the number of Compton-photoelectric events as a function of $\tilde{r}$, where $\tilde{r}$ is the perpendicular distance from the primary γ ray to the center of intensity of the light produced. All curves are normalized to equal counting efficiency, since their purpose is to show only the image resolution. For a 1/2-inch-thick crystal, $\tilde{r}$ is within the interval 0 to 0.1 inch for more than 90% of the photopeak events at the three γ-ray energies 0.28 MeV, 0.36 MeV, and 0.66 MeV. For a 2-inch-thick crystal, a considerable number are outside this interval, particularly at the higher energies.

Conclusions reached from Figs. 10 and 11 are that good position resolution can be obtained from 1/2-inch-thick crystals at all γ-ray energies, but high detection efficiency can be obtained only at the lower energies. For thick crystals, high detection efficiency can be obtained at high energies, but the position resolution is appreciably reduced by multiple scattering.

The results of these calculations are applicable to mosaics of sodium iodide crystals when no γ-ray shielding is employed between elements. When shielding is employed, many of the photopeak events will be reduced to ordinary Compton events as far as light output is concerned. If anti-coincidence circuitry is employed to reject Compton-photoelectric events that produce scintillations in two different elements of the mosaic, the effective detection efficiency will be reduced by elimination of these events.

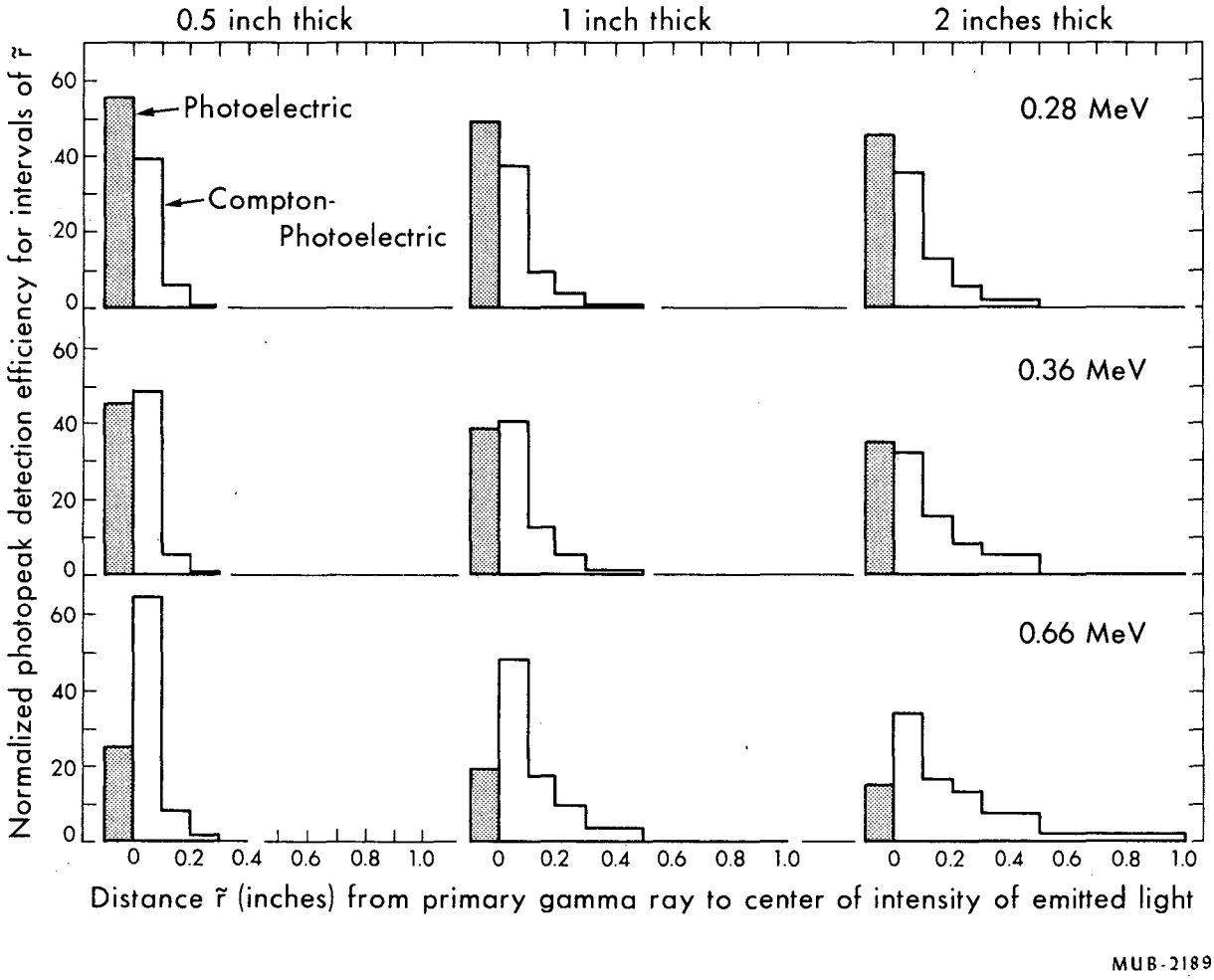

Fig. 11. Calculated loss of position resolution in sodium iodide due to multiple Compton-photoelectric interactions. The curves show the relative number of events occurring within intervals of $\tilde{r}$, where $\tilde{r}$ is the distance from the incident γ ray to the center of intensity of the light produced. Curves for 0.5-1-, and 2-inch-thick crystals at three γ-ray energies are shown (10).

Furthermore the smaller the area of the mosaic elements, the lower the effective detection efficiency will become.

The photopeak detection efficiency has been measured experimentally for a solid 0.46-inch-thick by 11.5-inch-diameter sodium iodide crystal by counting calibrated sources of Ce^{139}, Hg^{203}, I^{131}, Ge^{68}, and Cs^{137} at known geometry. The pulse-height selector was set to accept nearly all the photopeak as shown in Fig. 8O. The results, together with calculated efficiencies for a 0.46-inch-thick crystal, are shown in Table I. The actual counting efficiency is somewhat less than the calculated efficiency, probably because photopeak pulses at the upper and lower limits of amplitude were not accepted by the pulse-height selector window. A small loss was also caused by escape of recoil electrons from the surface of the scintillator.

2. Accuracy of Reproduction of the Scintillator Image on the Readout Oscilloscope

Mallard and Myers (43) have calculated the theoretical light collection of a seven-phototube array and showed that a nearly linear relationship exists between the position of each scintillation and the X and Y coordinate signals obtained fron the difference circuits. However, the calculations were based on a simplified model, because it is difficult to take into account the effect of light reflections from the diffuse white surfaces that surround the crystal and the phototubes and the effect of multiple internal reflections in the high-refractive-index crystal.

No method has yet been described to accurately calculate the optimum parameters of the image detector. These parameters include the distance between phototubes and crystal, the shape of the light deflector,

Table I. Calculated and measured photopeak detection efficiency for 0.46-inch-thick sodium iodide.

Isotope	γ-Ray energy	Calculated photopeak detection efficiency	Measured photopeak detection efficiency
Ce^{139}	0.166 MeV	89%	75%
Hg^{203}	0.28	39%	34%
I^{131}	0.36	26%	22%
Ga^{68}	0.51	15%	13%
Cs^{137}	0.66	10.4%	10%

the surface treatment of the crystal, etc. The methods used to develop the present image detectors were empirical.

The accuracy with which phototube-array cameras can determine the position of scintillations in the crystals is limited by the statistics of electron production in the phototubes. The loss of resolution from this cause is inversely proportional to the square root of the brightness of the scintillation. This is the reason that the phototube-array scintillation camera cannot be used for very-low-energy γ rays. A 27-keV γ ray from I^{125}, for instance, releases only about 27 electrons from all the photocathodes of the phototubes combined. When this small number of electrons is divided among the nearby phototubes, large statistical variations result, and positioning accuracy is poor.

Because of the foregoing limitation, and because of the problems of collimating high-energy γ rays, the useful energy range of the scintillation camera is considered to be from about .07 to 0.4 MeV, although lower-energy γ rays can be used with some loss of resolution, and also γ rays up to 0.7 MeV can be used at relatively low efficiency. Specially designed tungsten alloy collimators improved the efficiency at high energies.

A test picture showing the inherent resolution obtained at 0.36 MeV with the 19-phototube image detector is shown in Fig. 12A. An array of tungsten bars was placed 0.5 inch from the image detector. The size and spacing of the bars is shown in Fig. 12B. A point source of 0.36-MeV γ rays was located a few distant on the axis of the detector. Near the center of the picture, the 7/32-inch bars are clearly resolved and the 3/16-inch bars are barely resolved. The 1/4-inch bars are also resolved in the more difficult area at the edge of the picture. Since the useful area of

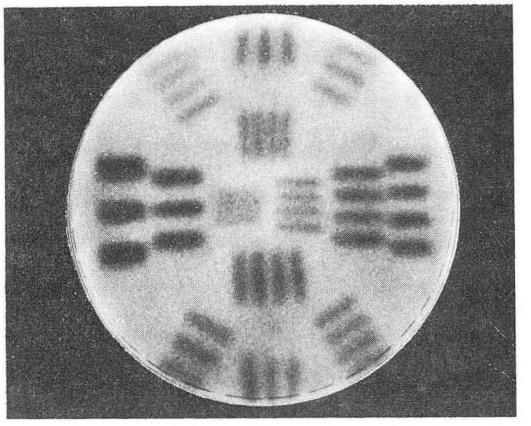

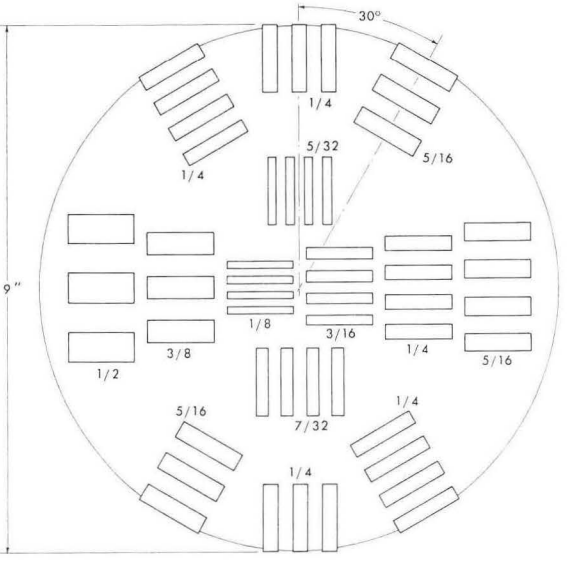

ZN-4776

Fig. 12. (A) Gamma-ray shadow picture of absorber bar pattern, demonstrating inherent resolution of 19-phototube image detector with 11.5-inch-diameter by 0.5-inch-thick scintillator. (B) Width of bars is equal to space between them, shown on diagram in inches.

the image detector is 9 to 10 inches in diameter, 1/4-inch resolution corresponds to more than 1,000 picture elements. Further tests show that the 1/4-inch bars can still be resolved in the central area at 0.16 MeV.

The linearity of image reproduction achieved with the 19-tube image detector is shown qualitatively in Fig. 13. These pictures were made by placing a radioactive "line source" at various positions under the camera and making multiple exposures. The line source consisted of a straight metal tube 12 inches long and 1/4 inch in diameter filled with a solution of positron-emitting Ge^{68}-Ga^{68}. Positron coincidence collimation was used and the source was 1 inch from the image detector housing in Fig. 13A and 3 inches away in Fig. 13B. The source was placed at 2-inch intervals to obtain the picture shown in Fig. 13B.

The pictures show that good linearity is achieved within an area 9 to 10 inches in diameter. Outside this area the scintillations are reproduced close together in an effect called "edge-packing." This effect is caused by the finite extent of the phototube array and reflection of light at the edges of the crystal.

D. Factors Affecting Background

In radioisotope cameras and scanners, background dots are caused by (a) cosmic rays, (b) radioactive materials and X-ray equipment in the vicinity of the instrument, (c) radioactivity in the internal parts of the detector, (d) γ rays from the patient that pass through the detector shielding and the walls of the collimator, and (e) scattering of γ rays in the subject.

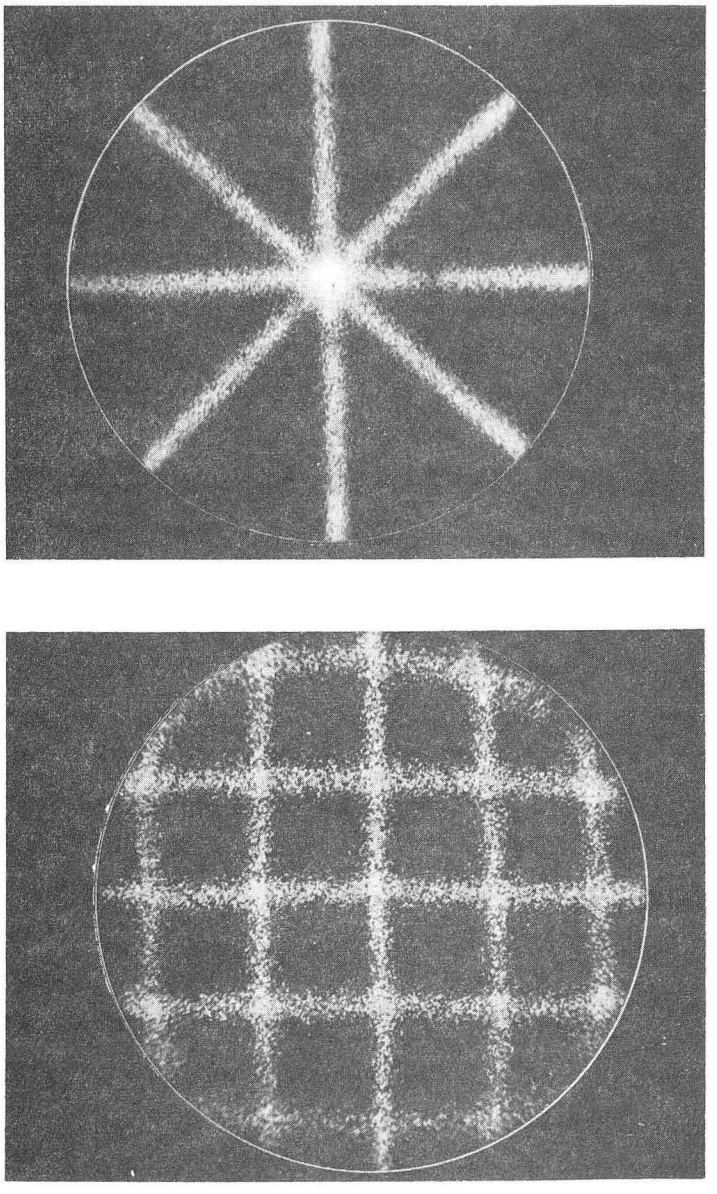

ZN-4778

Fig. 13. Test patterns showing linearity and resolution of 11.5-inch scintillator camera using line sources and positron coincidence collimation.

1. Stray Radiation

Causes (a), (b), and (d) above are of course minimized by adequate detector shielding and by the use of pulse-height selection. When tuned to 0.28-MeV γ rays, the scintillation camera described in Section IIB has a background of about 200 dots per minute under normal conditions. Massive shielding cannot reduce the background much below this value, because presently available phototubes contain radioactive substances (K^{40} and radium) in the glass and other parts. Also some cosmic rays pass through any practical amount of shielding.

2. Scattered γ Rays and their Rejection by Pulse-Height Selection

When the image detector is well shielded and the amount of radioactive material administered to the patient is adequate, the main cause of background dots is Compton scattering of the γ rays in surrounding tissue. When scattering occurs, any resulting dot in the picture is located at a position corresponding to the point of scattering, rather than to the point of origin of the primary γ ray. Medium-energy γ rays average 2 to 3 inches travel in soft tissue before being scattered. Therefore, γ-ray scattering in soft tissue produces a diffuse 2- to 3-inch-wide halo of dots around the active parts of the subject.

Compton scattering occurs in roentgenography, but in this case most of the secondary radiation is absorbed by slit filters aligned parallel to the primary x-ray beam (Potter-Bucky filter). Also the number of scattered x rays is minimized by limiting the width of the x-ray beam to the area to be imaged. However, these techniques can not be used when imaging the distribution of γ-ray-emitting isotopes. The only useful method for eliminating some of these scattered γ rays is pulse-height selection--determining

the energy of the detected γ ray and allowing it to be shown on the picture only if it has the same energy as the original γ rays of the particular isotope being used. This technique has been used in radioisotope scanners for many years (1).

However, not all scattered γ rays can be eliminated by pulse-height selection, because when a γ ray is scattered through a very small angle, the energy of the secondary γ ray is nearly equal to the original. The pulse-height-selector window must have a finite width in order to accept most of the photopeak, so an appreciable change in energy must occur to cause rejection of the secondary γ rays.

The situation is worse at low γ-ray energies because the secondary γ rays retain more of the original energy, and at the same time a wider pulse-height selector window must be used because the pulse-height resolution of scintillation detectors decreases at low energies. Also, more Compton scattering occurs at lower energies.

The energy retained by Compton-scattered γ rays can be easily calculated (25). Also, the angular distribution of the secondary γ rays can be determined from the Klein-Nishina formulas (23). Because multiple scattering occurs, an accurate calculation of the fraction of scattered γ rays removed by pulse-height selection at different primary γ-ray energies requires complex calculations such as Monte Carlo methods. However, a rough indication of the fraction of scattered γ rays removed by pulse-height selection can be obtained from single-hit calculations, the results of which are shown in Fig. 14. These calculations assume a radioactive source 3 inches below the surface of soft tissue and a pulse-height-selector

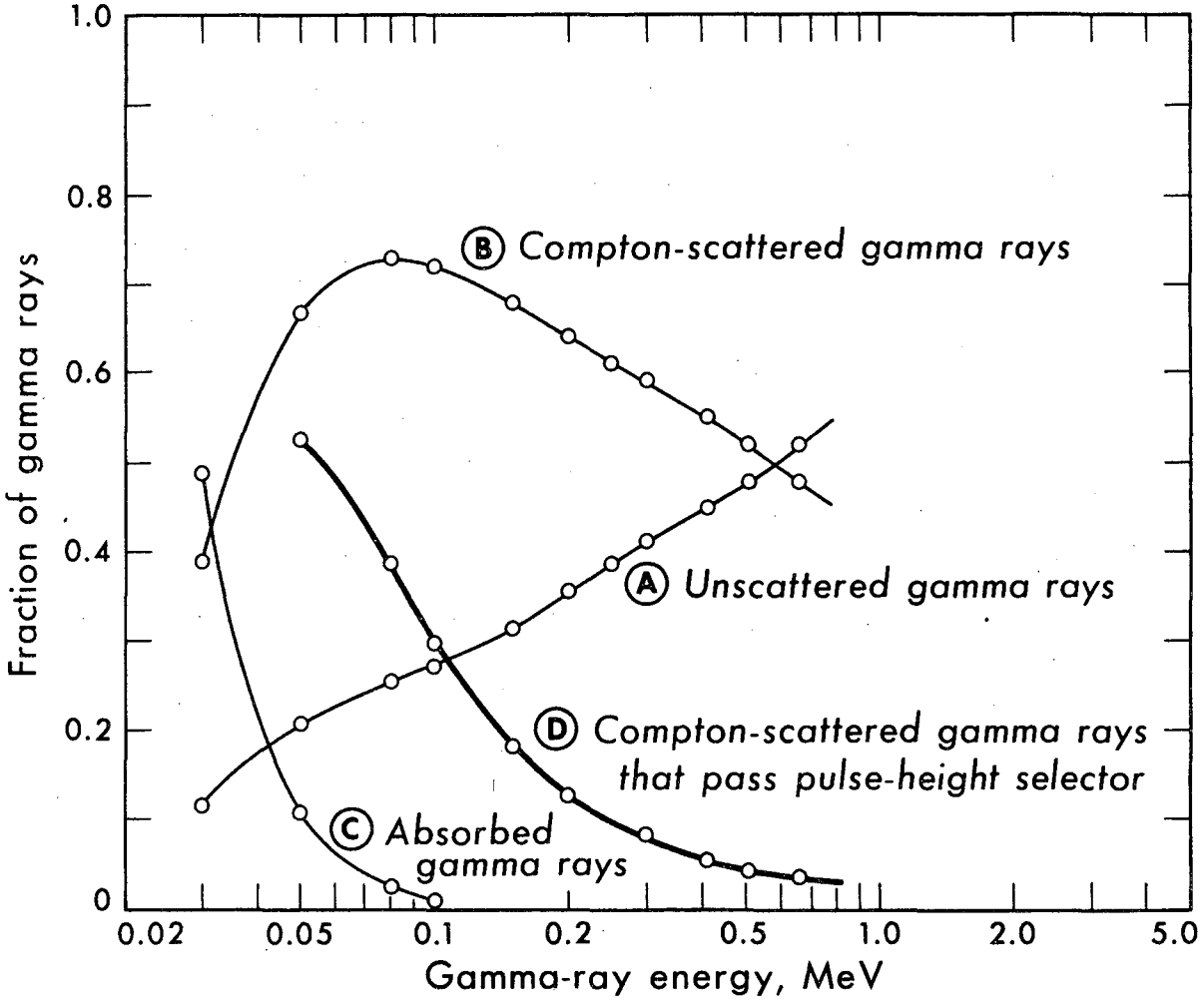

Fig. 14. Fraction of γ rays from source 3 inches below tissue surface that (A) escape unscattered and unabsorbed, (B) escape but have been Compton scattered, (C) are absorbed and do not escape the surface of the tissue, and (D) are Compton scattered but not removed by pulse-height selector as described in text.

window whose lower edge is set according to the pulse-height resolution expected at various energies. It was 9% under the primary γ-ray energy at 0.66 MeV and 20% under at 0.10 MeV. Intermediate values were based on assumption of a linear relationship between the lower edge and $(1/E)^{1/2}$, where E is the primary energy of the γ ray.

Reference to the curves in Fig. 14 shows that at 0.36 MeV, 43% of the γ rays escape the subject without scattering or absorption (curve A) and 57% are Compton-scattered (curve B). All the latter will be shown on the picture if pulse-height selection is not used. If pulse-height selection is used, only 6% of the original γ rays will be Compton-scattered and shown on the picture (curve D). None of the γ rays is totally absorbed in the subject at this energy (curve C).

Thus, the usefulness of pulse-height selection at this medium γ-ray energy is apparent, because there is a factor-of-10 reduction in scattered γ-ray background. At lower energies, pulse-height selection is of less value, as the curves show. More scattering occurs, and pulse-height selection is less able to remove it. However, if multiple scattering were taken into account in the calculations, more improvement would be shown at the lower energies.

III. IMAGE-PRODUCING COLLIMATORS FOR USE WITH GAMMA-RAY EMITTERS

Three different methods of collimation can be used to project images of radioactive subjects onto a scintillator. They are pinhole collimation and multichannel collimation for γ-ray emitters, and coincidence collimation of annihilation radiation for positron emitters. The first two methods are discussed in this section and the third is discussed in Section IV.

A. Pinhole Collimators

A pinhole collimator consists of a shallow aperture at the end of a lead shield, as shown in Fig. 2. Gamma rays that enter the aperture continue traveling in straight lines to form an inverted image of the subject at the scintillator. Characteristics of pinhole collimation include the following. Subjects of nearly any size can be accommodated by placing them close to or far from the aperture. Magnified images of small subjects can be projected onto the scintillator to provide high resolution. The aperture size can be easily changed to provide the best compromise between sensitivity and resolution. Also, pinhole collimators produce images that have no distorting patterns superimposed, because each point in the subject is imaged as a small circular area on the scintillator.

The geometric resolution and efficiency of single-aperture pinhole collimators have been discussed in previous publications (6,43,46). Briefly, the geometric resolving distance of a pinhole collimator is given by

$$R = \frac{(a + b)\, d_e}{a} ,$$

where a is the distance from the aperture to the scintillator, b is the distance from the subject to the aperture, and d_e is the

effective diameter of the aperture. The resolving distance R is defined as the distance between two point sources in the subject that are imaged as two discs that are tangent at the scintillator. The above equation does not take into account any resolution subsequently lost in the translation of the γ-ray image into a picture.

The effective diameter d_e of a pinhole aperture is somewhat larger than the actual diameter d, owing to penetration of the edges of the aperture by γ rays. To reduce scattering of the γ rays, the apertures are usually made of tungsten, platinum, or other high-density material. Table II gives the actual and effective diameters of typical apertures in lead, tungsten, and platinum at several γ-ray energies.

The goemetric efficiency g of a pinhole collimator is given by

$$g = \frac{d_e^2}{16\, b^2},$$

where g is defined as the fraction of γ rays emitted by the subject that pass through the aperture.

The overall sensitivity S in terms of the number of dots per minute recorded on the picture per microcurie of activity in the subject, neglecting absorption in the subject, is given by

$$S = 2.2 \times 10^6 \, \epsilon \, f_a \, \frac{d_e^2}{16\, b^2},$$

where ϵ is the photopeak detection efficiency of the scintillator and f_a is the abundance factor of the γ ray, or the average number of γ rays of a given energy emitted per disintegration.

Table II. Effective diameter d_e for apertures with 60-deg angle of view (inches).

Actual diameter (inches)	Aperture material	γ - Ray energy (MeV)						
		0.14	0.20	0.28	0.36	0.41	0.51	0.66
0.125	Pb	0.134	0.146	0.171	0.199	0.220	0.260	0.315
	W	0.132	0.141	0.158	0.179	0.195	0.219	0.250
	Pt	0.130	0.138	0.152	0.171	0.179	0.201	0.231
0.187	Pb	0.196	0.208	0.223	0.261	0.282	0.322	0.377
	W	0.194	0.203	0.220	0.241	0.257	0.281	0.312
	Pt	0.192	0.200	0.214	0.233	0.241	0.263	0.293
0.250	Pb	0.259	0.271	0.296	0.324	0.345	0.385	0.440
	W	0.257	0.267	0.283	0.304	0.320	0.346	0.375
	Pt	0.255	0.263	0.277	0.296	0.304	0.326	0.356

Pinhole collimation provides the best combination of sensitivity and resolution for small subjects if they can be positioned a few inches from the aperture. The thyroid gland is an example. Five microcuries of I^{131} located 3 inches from a 3/16-inch-diameter tungsten aperture typically produces about 500 dots per minute on the picture if the scintillator is 0.5-inch-thick sodium iodide. Calculations and actual measurements of the sensitivity agree. The area of the subject seen by the camera, assuming a 60-deg angle of view, is a 3.5-inch-diameter circle.

When a conventional 61-hole focused-collimator scanner is used to scan an equivalent area, an average of 130 counts per minute is detected. Therefore the scintillation camera requires 1/3 the exposure time for an equal number of γ rays to be recorded. Equal resolution is obtained by the two methods, as determined by comparing pictures of human subjects and thyroid phantoms.

Although pinhole collimators are most efficient for small subjects, they can also be used to take pictures of very large subjects, such as the entire lung or a grossly enlarged liver, when a large enough quantity of isotope is present. After obtaining an overall picture, the camera can be moved closer to take high-resolution pictures of smaller areas.

B. Pinhole Collimators With More Than One Aperture

For some purposes, pinhole collimators with more than one aperture can be effectively used (8,14). For the thyroid gland, three apertures provide three different views of the gland simultaneously when the apertures are suitably positioned and they are used with a large image detector. A section drawing of this collimator is shown in Fig. 15A. The central aperture

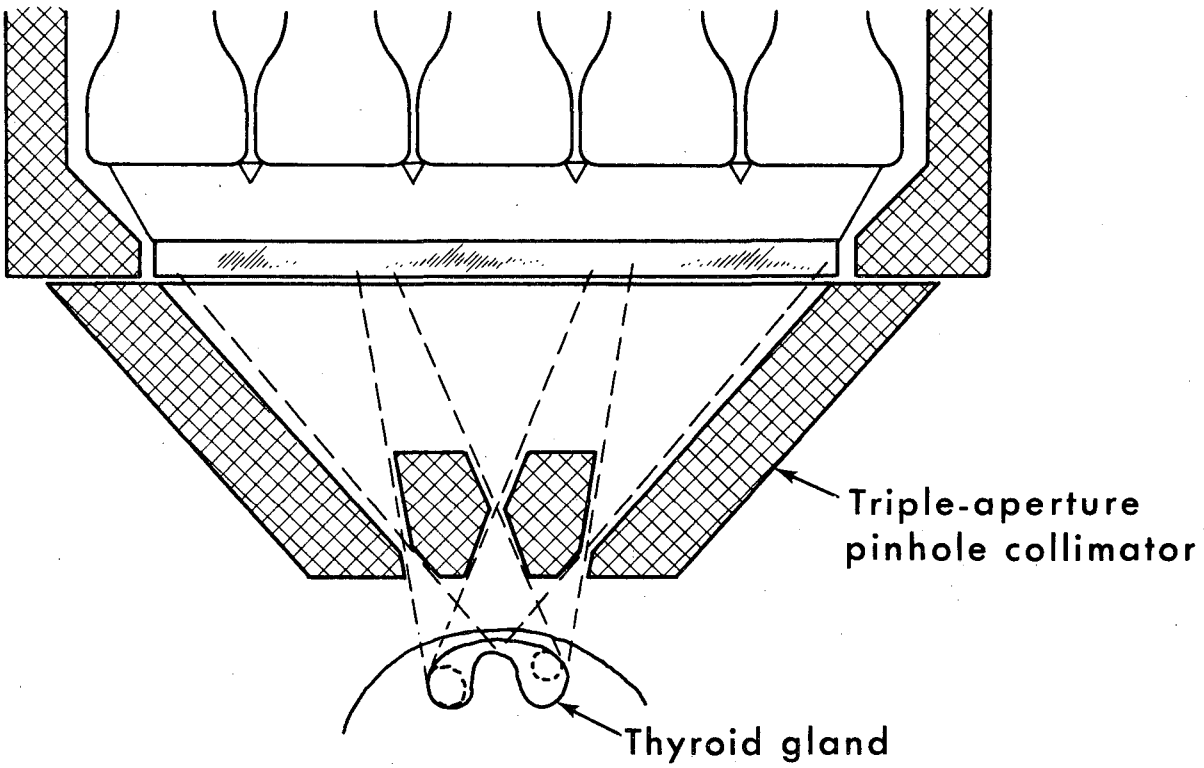

Fig. 15. (A) Section view of triple-aperture pinhole collimator used for imaging the thyroid gland. (B) Three complete γ-ray images of the gland are projected, but the image detector crystal intercepts only half of the two side images.

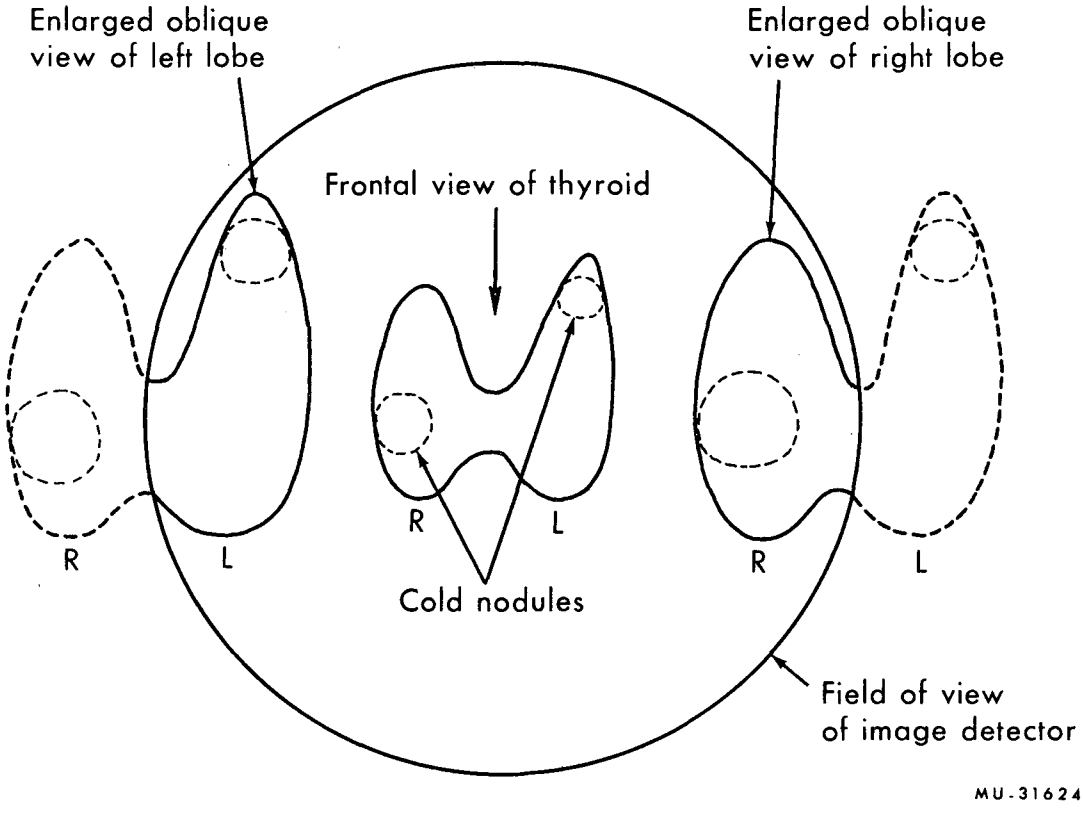
Enlarged oblique
view of left lobe
Enlarged oblique
view of right lobe
Frontal view of thyroid
R
L
R
L
R
L
Cold nodules
Field of view
of image detector
MU-31624

Fig. 15b

projects a conventional view of the entire thyroid gland on the central portion of the scintillator. At the same time, the left aperture projects an enlarged oblique view of the left lobe on the left portion of the scintillator. The view is enlarged because the left aperture is closer to the subject than the central aperture. The right aperture projects a similar view of the right lobe on the right portion of the scintillator.

As shown in Fig. 15B, three complete γ-ray images of the thyroid are produced by the three apertures, but the scintillator, represented by the circle, intercepts only one-half of the two side images. This arrangement provides increased chances of seeing a nodule in or near the thyroid because each lobe is viewed from two different angles. Also, increased resolution is obtained in the two enlarged views. Furthermore, it is possible to determine whether specific areas of tissue are anterior or posterior to the gland by observing a shift in relative position of the tissue in the different views.

Pictures taken with the triple-aperture collimator are shown in Fig. 16. Exposure times are typically 5 to 10 minutes with 5 to 10 μC of I^{131} in the gland.

C. Multichannel Collimators

A multichannel collimator consists of a plate made of γ-ray-absorbing material with hundreds or thousands of channels through it. Each channel accepts γ rays from only a limited area, and a γ-ray image of the subject results at the exit side of the collimator. This type of collimator has been discussed in detail in an earlier publication by the author (11).

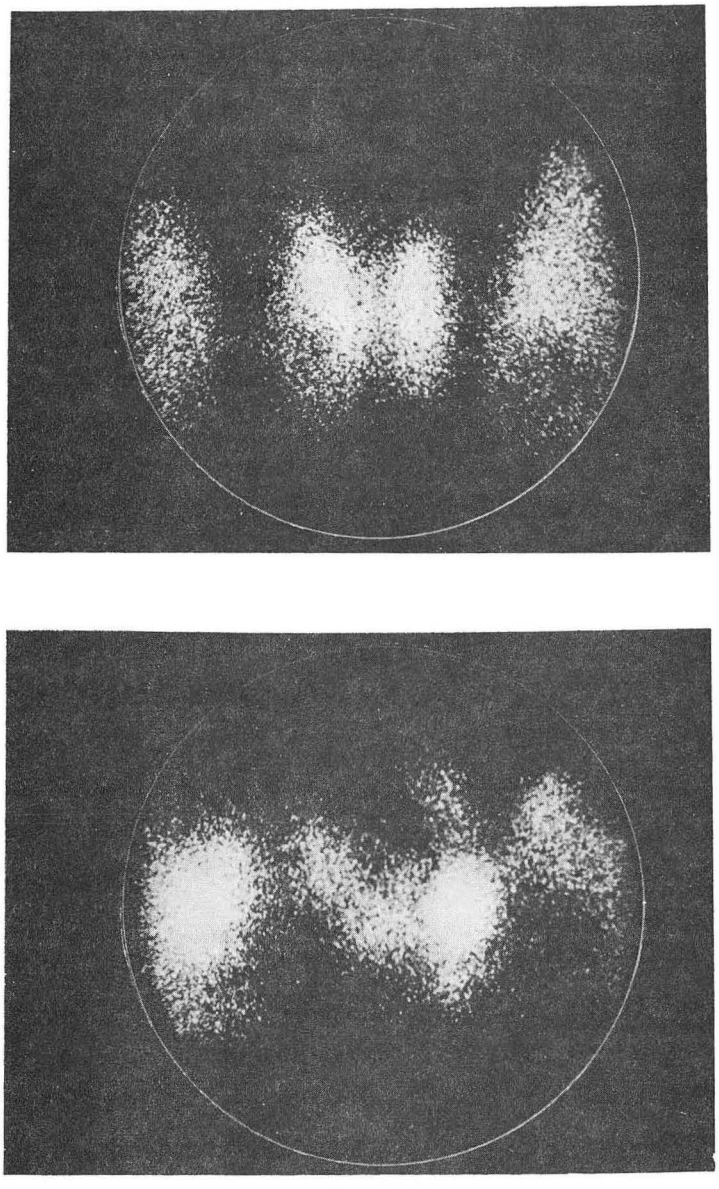

(a)

(b)

ZN-4784

Fig. 16. Triple-aperture pinhole pictures of thyroid gland. (A) Cold nodule is seen most clearly in oblique view at right. (B) Small amount of active tissue above the patient's left lobe in frontal view is not visible in oblique view at left. This indicates tissue is considerably anterior or posterior to the rest of the gland.

The scintillation camera image detector is shown with a typical parallel-channel collimator in Fig. 6. In normal use the subject is located as close as possible to the entrance side of the collimator. Compared to pinhole collimators, multichannel collimators provide the best combination of sensitivity and resolution for large organs such as the brain, liver, and heart.

Characteristics of Multichannel Collimators

Collimators with parallel channels have the following characteristics. The size of the image is independent of the distance from subject to collimator. This is an advantage when an organ lies at an unknown depth and its size is to be determined. There is substantially uniform "depth response" in air. In other words, the same counting rate is obtained whether the subject is close to the collimator or distant, as long as the subject is imaged completely within the boundaries of the scintillator. Of course the depth response in tissue is modified by absorption and scattering.

The resolution of parallel-channel collimators is best for the parts of the subject closest to the collimator, and the resolution decreases with increasing distance from the collimator. In comparison, the resolution of focused collimators used for scanning is best for the parts of the subject at the geometric focus, which is usually 3 inches from the collimator. Their depth of focus is limited, and planes closer and farther away are less sharply resolved (21, 23). However, parallel-channel collimators can be designed to have the same geometric resolution at a distance of 3 inches as the typical focused collimators used for scanning. Then the parallel-channel collimator will have greater depth of focus, because it will sharply resolve all the closer planes, whereas the focused collimator will not. Because clinical

subjects are nearly always several inches thick, the "depth of focus", or the depth over which a relatively sharp image is obtained, should be taken into account in evaluating any collimation method.

Design of Multichannel Collimators

Multichannel collimators can be made with many combinations of hole diameter, length, and septal thickness. The formulas given in the next paragraphs assist in designing parallel-hole straight-bore collimators that have maximum efficiency for a given resolution and maximum γ-ray energy.

The mathematical analysis of this type of collimator is simplified if the assumption is made that the collimator moves sideways in the manner of a Potter-Bucky filter during the exposure time. The formulas have been derived by (a) assuming that the collimator moves relative to the subject and image detector during the exposure time, (b) determining the fraction of the time that a point source in the subject is visible to each element in the image detector, (c) determining the solid angle from the source to each element, and (d) integrating to obtain the overall counting efficiency.

For example, consider a collimator consisting of a rectangular array of square holes as shown in Fig. 17. This section view shows a plane through the center of a row of holes. The width of the holes is d, the length is a, and the septal thickness is t. The distance from the radioactive subject to the entrance of the collimator is b, and the distance from the exit to the central plane of the scintillator is c.

If the collimator is stationary, the distribution of γ rays has the irregular shape shown at the top of Fig. 17, but if the collimator moves in the direction shown, the average distribution of γ rays that strike the scintillator has the triangular shape shown immediately above the scintillator.

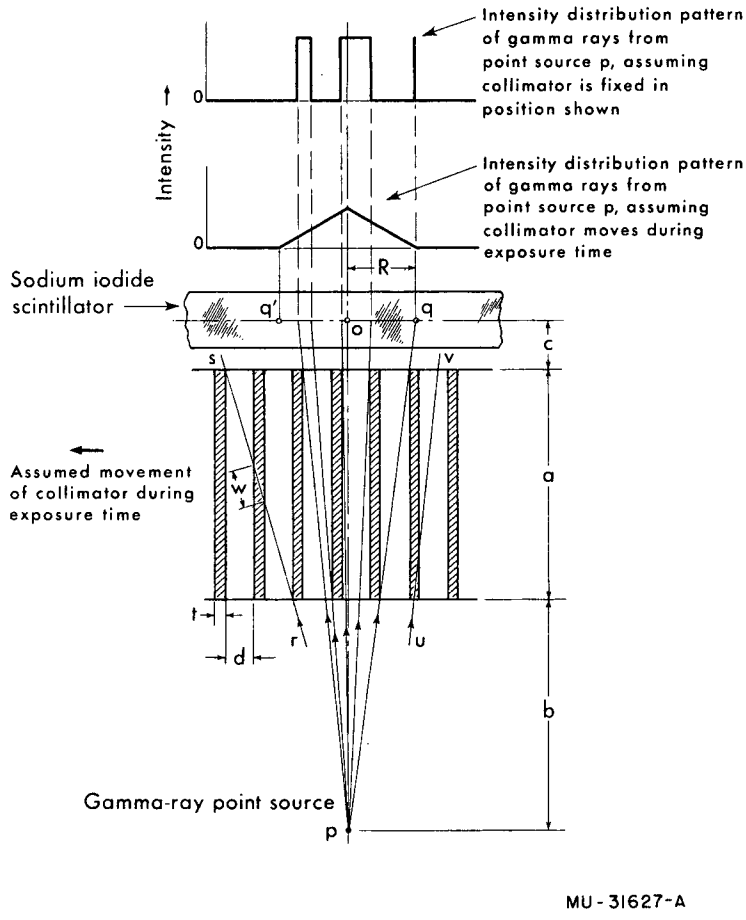

Fig. 17. Section view of multichannel collimator. Gamma-ray pathways are shown at bottom, irradiated areas of scintillator when collimator is stationary at top, and irradiated area if collimator moves during exposure time at center (11).

The intensity is a maximum at point o directly above the point source, and it falls linearly to zero, assuming opaque septa, at points q and q'. The distance oq, which is equal to the full width of the triangular-shaped intensity curve at half maximum, is defined as the geometric resolving distance R.

From geometric considerations, it can be shown that

$$R = \frac{d(a_e + b + c)}{a_e} .$$

As expected, the resolving distance R is smallest, or in other words the image is sharpest, when the distances b and c are small. The effective length of the collimator is less than the geometric length because γ rays penetrate the edges of the collimator material, taking the path μv in Fig. 17. It has been shown (45) that the effective length of the collimator holes a_e is approximately given by

$$a_e = a - 2\mu^{-1} ,$$

where μ^{-1} is the mean free path of the γ ray in the material and μ is the total linear absorption coefficient (25,34). Values of μ^{-1} in lead and tungsten are listed for several γ-ray energies in Table III.

The geometric efficiency is given by

$$g = \left[\frac{Kd^2}{a_e(d+t)} \right]^2 ,$$

where g is defined as the fraction of γ rays emitted by the subject that pass through the collimator channels. Gamma rays that are scattered by the channel walls and any that travel through the septa are not included.

Table III. Values of μ^{-1}, mean free path of γ rays in collimator material (in inches). Density of Pb = 11.4 g/cm^2; Density of W alloy = 18.5 g/cm^2. Values of μ interpolated from reference 34.

		γ-Ray energy (MeV)					
		0.14	0.20	0.28	0.36	0.41	0.66
μ^{-1}	Pb	0.0144	0.036	0.078	0.128	0.164	0.33
	W alloy	--	0.0284	0.059	0.095	0.118	0.224

The value of the constant K depends on the shape of the holes and their distribution pattern. It has been determined mathematically and confirmed approximately by experiment that K = 0.282 for square holes in a rectangular array and K = 0.238 for round holes in a hexagonal array. Inspection of the previous equation shows that g is independent of b, the distance between the subject and the collimator, providing the subject is completely imaged within the boundaries of the scintillator. Therefore, parallel-channel collimators should have uniform "depth response" in air, or in other words the counting rate of a subject in air should be independent of the distance from the collimator to the subject. This has been found by experiment to be approximately true.

The shortest distance a γ ray can travel through septal material when taking the unwanted path of minimum attenuation rs, shown in Fig. 17, is w. From experimental studies, acceptable images result when the narrow-beam (Compton + photoelectric) attenuation of γ rays taking the path rs is 95% or more. Since $1 - (1/e)^3 = 0.95$, w is equal to 3 times the mean free path of γ rays in the collimator material, or $w = 3\mu^{-1}$. Values of μ^{-1} are given in Table III for lead and tungsten-alloy. With w known, the minimum permissible septal thickness t can be calculated for any hole diameter and length. For geometric considerations,

$$t = \frac{2dw}{a - w} .$$

The sensitivity S in terms of dots per minute recorded on the picture per microcurie of activity in the subject, neglecting absorption in the subject, is given by

$$S = 2.2 \times 10^6 \, f_a \epsilon \, \frac{Kd^2}{a_e^2 \, (d + t)^2}$$

where ϵ is the photopeak detection efficiency of the scintillator, and f_a is the abundance factor or the average number of γ rays of a given energy emitted per disintegration. Values of ϵ are given in Section II C1. With the above equations, collimators can be designed that have optimum hole diameter, length, and septal thickness for a given subject-to-collimator distance, maximum γ-ray energy, and desired resolution.

The parameters of five typical collimators designed for maximum efficiency consistent with the stated resolving distance and maximum γ-ray energy are given in Table IV. The material is lead, and all have hexagonal arrays of round holes. The calculated overall sensitivity in terms of dots per minute per microcurie takes into account the abundance factors of the principal γ rays. The Compton contribution of the high-energy components of I^{131} was not included. The increase in resolving distance R and the increase in geometric efficiency because of γ rays penetrating the edge of the collimator material were taken into account in the calculations.

Other calculations indicate that higher sensitivity can be achieved if the collimators are made of tungsten alloy. The improvement results from having thinner septa and therefore more holes of the same diameter per unit area. The increase in sensitivity varies from 21% for collimators designed for 0.28 MeV maximum to 30% for those designed for 0.41 MeV.

When an organ such as the kidney is imaged with Collimator No. 3 of Table IV, calculations indicate that 25 μC of Hg^{203} in the organ should produce 2800 dots per minute on the picture, assuming that 50% of the γ rays are absorbed by 7 cm of overlying tissue. This is the approximate counting

Table IV. Parameters of five typical collimators, designed for maximum efficiency consistent with stated resolving distance and maximum γ-ray energy.

Collimator number			1	2	3	4	5
Nominal maximum γ-ray energy (MeV)			0.20	0.28	0.28	0.36	0.41
Hole length, a (in.)			1.0	1.5	1.5	2.2	2.6
Hole diameter, d (in.)			0.111	0.225	0.150	0.193	0.213
Septum thickness, t (in.)			0.030	0.094	0.063	0.089	0.106
Number of holes in 11-in.-diam area			5600	1090	2450	1400	1090
Tc^{99m} (0.14 MeV)	Calculated dots/min/μC		890	1080	746	336	282
	Resolving distance, R (in.),	at b=1 in.	0.28	0.47	0.30	0.32	0.34
		at b=3	0.51	0.76	0.51	0.50	0.50
		at b=5	0.74	1.07	0.71	0.68	0.67
Hg^{203} (0.28 MeV)	Calculated dots/min/μC		---	500	224	137	121
	Resolving distance, R (in.),	at b=1 in.	---	0.48	0.32	0.33	0.34
		at b=3	---	0.82	0.54	0.52	0.52
		at b=5	---	1.15	0.77	0.72	0.69
I^{131} (0.36 MeV)	Calculated dots/min/μC		---	---	---	101	80
	Resolving distance, R (in.),	at b=1 in.	---	---	---	0.34	0.35
		at b=3	---	---	---	0.54	0.53
		at b=5	---	---	---	0.75	0.72
Au^{198} (0.41 MeV)	Calculated dots/min/μC		---	---	---	---	83
	Resolving distance, R (in.),	at b=1 in.	---	---	---	---	0.35
		at b=3	---	---	---	---	0.54
		at b=5	---	---	---	---	0.73

obtained in practice. Clinically satisfactory picture containing about 15,000 dots are obtained in 5 minutes.

An example of a brain tumor picture taken with a multichannel collimator similar to No. 2 in Table IV and designed for 0.28 MeV maximum is shown in Fig. 18. The patient was given 700 μC of Hg^{203} Neohydrin, and 4 hours later the pictures showing (A) left lateral and (B) back views were taken. The exposure time was 5 minutes each and 25,000 dots were recorded. A tumor is visible in the region at left of midline. Two small radioactive marker sources were placed at the corner of the eye and the bottom of the ear lobe for the lateral view, and at the ear canals in the back view. An outline of the head due to body background is also seen. The field of view of the camera is indicated by the circular line. The collimator used for this case is equivalent to the conventional 19-hole focused collimators used for scanning, having relatively high efficiency and moderate resolution.

Pictures of a brain tumor in another patient taken with 2 mC of Tc^{99m} as the pertechnetate ion are shown in Fig. 18C. Exposure times were 3 minutes each, and about 200,000 dots were recorded on each picture.

Large amounts of Tc^{99m} can be given without excessive radiation dosage to the patient because the half life is short (6 hours) and no β particles are emitted (36). The energy of the emitted γ ray is 0.14 MeV. The Tc^{99m} is obtained from a parent nuclide Mo^{99}, which has a half life of 2.8 days.

The collimator used for the foregoing study was specially designed for use with low-energy γ rays, and was made of lead foil and balsa wood. The balsa wood aided in fabrication of the array of 4000 square holes (11) and was left in place because it added strength and absorbed few γ rays.

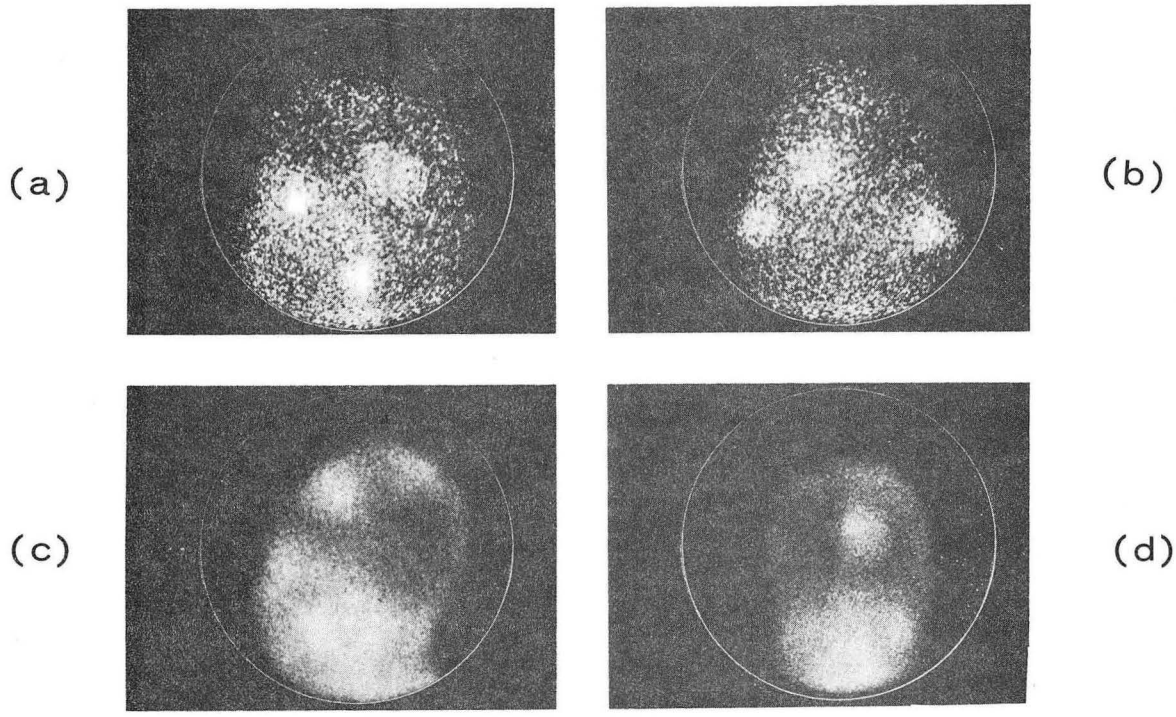

Fig. 18. (A) Left lateral and (B) posterior views of a brain lesion taken with a multichannel collimator designed for nominal maximum γ-ray energy of 0.28 MeV. The tracer was 700 μC of Hg^{203} Neohydrin. A prominent lesion and two small marker sources are seen in each view, as well as an outline of the head due to body background. Exposure time was 5 minutes per view. (C) Left lateral and (D) frontal views of a brain lesion taken with 0.14-MeV γ-ray emitter Tc^{99m}. Two mC of the pertechnetate, which distributes in extracellular fluid space, was administered, and pictures were taken a few minutes later. Duration of exposure was 3 minutes each. A multichannel collimator designed for 0.20-MeV maximum γ-ray energy was used.

With this collimator about 1000 dots per minute are obtained per μC of Tc^{99m}, neglecting absorption in the subject. This high sensitivity is due partly to the high detection efficiency of the scintillator and partly to the high geometric efficiency of the collimator.

The kidneys of an adult patient are shown in Fig. 19A. In this case, higher resolution was desired so a collimator similar to No. 4, which is approximately equivalent to the conventional 37-hole focused collimator, was used. The patient received 100 μC of Hg^{203} Neohydrin, and the picture was taken 1 hour later. Exposure time was 5 minutes and the picture contains 30,000 dots.

The kidneys of a 9-year-old child are shown in Fig. 19B. In this case, dose reduction was desired, so the patient was given only 5 μC of Hg^{203} Neohydrin and the exposure time was increased to 15 minutes.

Both kidneys can be shown in one view of 90% of the patients examined (30). When the kidneys are too far apart or greatly enlarged, separate views are taken of each. Often lateral and anterior views are taken in addition to the conventional posterior views shown above. This procedure is made convenient by the short exposure times.

Pictures from a dynamic study of 10 mC of $Tc^{99m}O_4^-$ going through the heart of a normal human after rapid intravenous injection in the anticubital vein are shown in Fig. 20A. The scintillation camera viewed the anterior chest and pictures were taken at the rate of one frame per second on 16 mm motion picture film. In frame 3, taken 3 seconds after initial detection of activity in the heart, the active bolus is located in the superior vena cava and the right atrium and ventricle. In frame 5, taken at 5 seconds, more activity is seen in the main pulmonary artery, and at the top of the

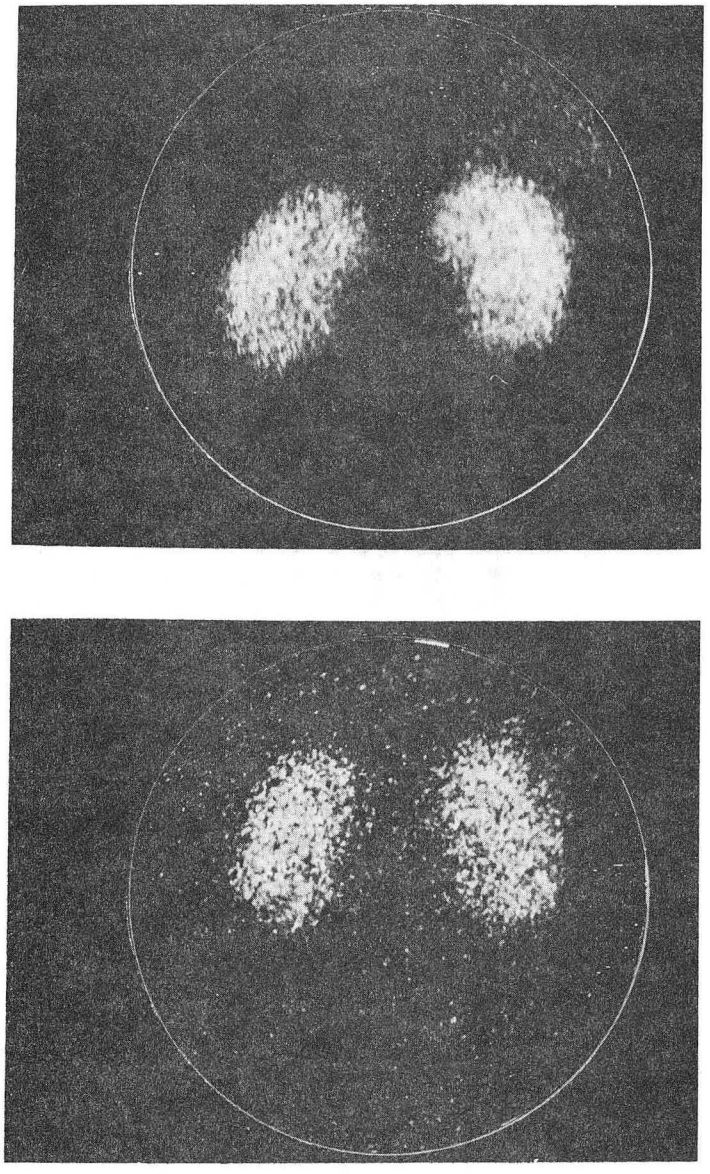

(a)

(b)

ZN-4786

Fig. 19. (A) Normal adult kidneys taken with multichannel collimator; 100 μC of Hg^{203} Neohydrin was given and exposure time was 5 minutes. (B) Kidneys of a 9-year-old child; to reduce radiation dose, only 5 μC of Hg^{203} Neohydrin was given and exposure time was 15 minutes.

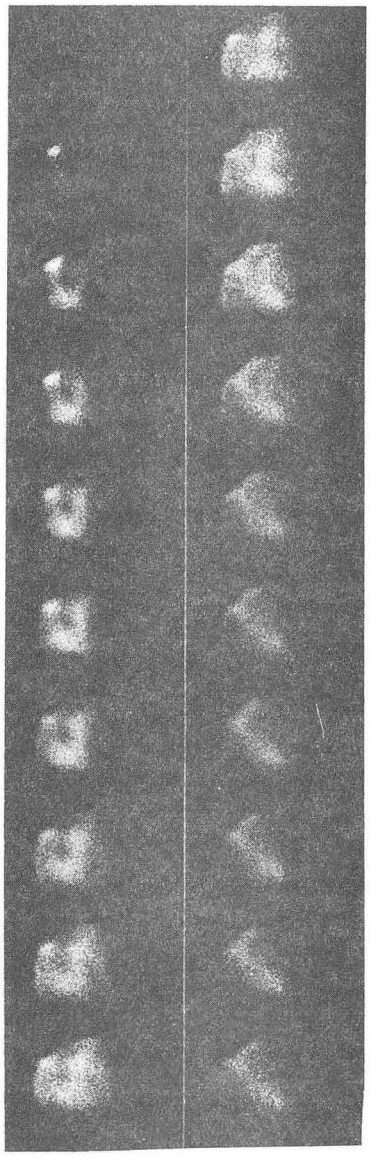

ZN-4782

Fig. 20. Stop-motion pictures of 10 mC of Tc^{99m} going through normal human heart. Isotope was injected into arm vein, and exposure time was 1 second per frame. Line drawings show interpretation of pictures at 3, 5, and 14 seconds after activity first appears in heart.

SCHEMATIC INTERPRETATION OF HEART SCINTIPHOTOS

Frame 3

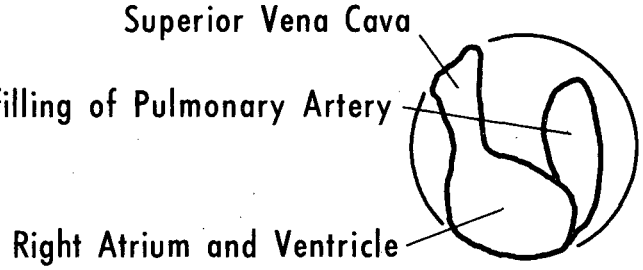

(b)

Frame 5

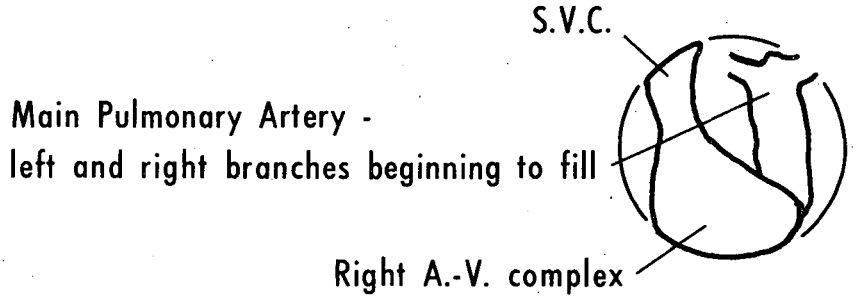

(c)

Frame 14

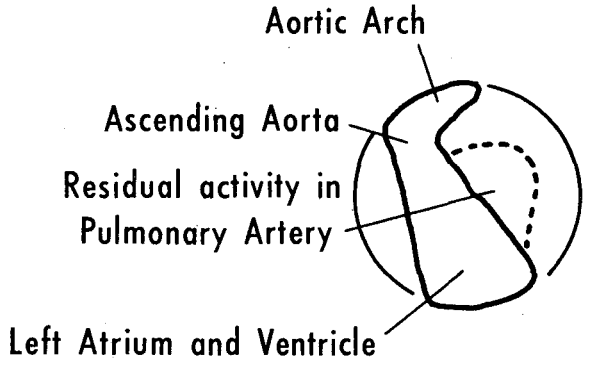

(d)

MUB-4464

Fig. 20b

picture a suggestion is seen of the right and left branches beginning to fill. In frame 4, taken at 14 seconds, the aortic arch, the ascending aorta, and the left atrium and ventricle are visible, as well as some residual activity in the pulmonary artery. Line drawings made from these interpretations are shown in Fig. 20B, C, and D.

IV. THE POSITRON CAMERA: COINCIDENCE COLLIMATION OF ANNIHILATION RADIATION FROM POSITRON EMITTERS

The instruments described in this section are special forms of radioisotope cameras for producing pictures of the distribution of positron-emitting nuclides (6, 8, 12, 15). Whenever a positron is stopped by matter, it combines with a negative electron and produces two 0.51-MeV annihilation γ rays that travel away from their point of origin at 180 deg. This property allows images to be formed with two detectors on opposite sides of the subject, coincidence circuitry, and electronic computation techniques. Conventional image-producing collimators, such as pinhole or multichannel collimators, are not required. The subject is placed as close as possible to the image detector, as shown in Fig. 7, and a second detector, called the focal detector, is located a distance below the subject.

Positron cameras have several unique properties. They have substantially uniform "depth response" in tissue, so that tumors deep within the body can be detected as easily as those on the surface. This is a unique property that can not be obtained from instruments that detect single γ rays. The background count rate in the absence of positron emitters is extremely low, only a few counts per hour. This permits taking long exposures of subjects containing very little activity. When both detectors have position-sensing capabilities, high sensitivity can be obtained in combination with sharp resolution on organs deep within the subject. A "plane of best focus" exists that can be set to any desired level by adjustment of an attenuator in the electronic circuits.

Positron cameras have the following disadvantages and limitations. First, they are complex instruments employing many components. Second, there is a limit to the amount of radioactive material than can be used with them; overload of the electronic circuits can occur because of the very high count rates produced, since there is no collimator between the image detector and the subject. However, the activity permitted before overload occurs in existing instruments allows pictures to be obtained with exposures as short as 1 minute. Third, the availability of positron emitters is limited, because most must be cyclotron-produced. Important exceptions are Ga^{68}, which is very easily obtained from a long-lived parent ( ), and F^{18} and Cu^{64}, which are reactor-produced. Moreover, some positron emitters have unique uses in biology and medicine for which no substitutes are available.

A. Types of Positron Cameras

Positron cameras can take several different forms, as described in the following paragraphs.

Unfocused Positron Cameras

In this relatively simple instrument, the same image detector described in Section II is employed, the subject is placed as close to the scintillator as possible, and a scintillation counter with a large thick crystal is located a distance away on the opposite side of the subject, as shown in Fig. 21A. When a γ-ray pair causes coincident scintillations in the two detectors, the scintillation in the image detector is displayed on the image-readout oscilloscope. Scintillations occurring in the image detector that are not in time-coincidence with a γ ray detected by the scintillation counter are not displayed.

The remote γ-ray counter is called a focal detector because all γ-ray pairs that form an image of the subject must impinge upon it, and therefore

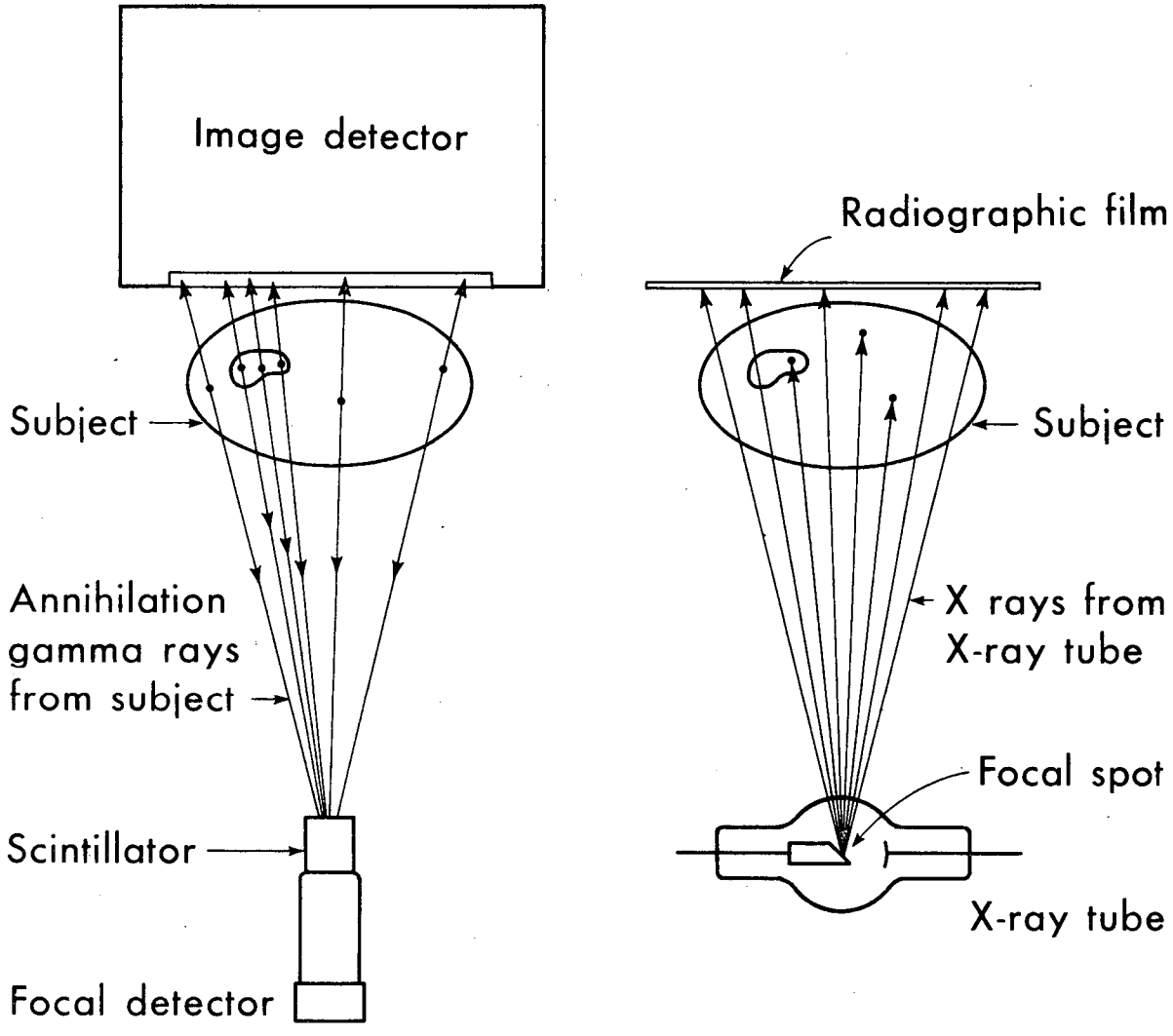

Fig. 21. (A) Positron camera with single remote γ-ray counter as focal detector. (B) Analogy between (A) and x-ray radiograph of same subject. Geometry of image formation in the two cases is the same.

it is a focal point in the image geometry. The geometry of image formation is analogous to x-ray radiography, as shown in Fig. 21B. The focal spot of the x-ray machine is equivalent to the focal detector, and the x-ray film is equivalent to the image detector. In x-ray radiography, the radiation originates in the x-ray tube and a fraction of the rays are absorbed by the subject. In positron imaging, the radiation orginates in certain areas of the subject, but since the radiation consists of γ-rays pairs traveling in opposite directions along straight lines and since all γ-ray pairs displayed on the image readout oscilloscope must pass through the focal detector, the geometry of image formation is the same. A slightly magnified image of the subject is "projected" on the image detector crystal.

Expressions for the resolution and sensitivity of this instrument are given in an earlier publication (6). The unfocused positron-camera has been superseded by the more sensitive focused types described in the following sections.

Twin-Image-Detector Focused Positron Camera. Another method of imaging positron emitters is to employ two identical image detectors located on opposite sides of the subject, as shown in Fig. 22A. Pulses from the two image detectors are sent to a coincidence circuit which responds only when simultaneous γ rays are detected. Activity lying on the central plane of the subject is shown with sharp resolution by taking a simple average of the x-coordinate signals from the two detectors and also an average of the y-coordinate signals. These new coordinate signals are sent to the deflection inputs of the image readout oscilloscope, and the output of the coincidence circuit is sent to the intensity input. The beam of the cathode-ray tube is positioned by the averaged x and y signals and is turned on

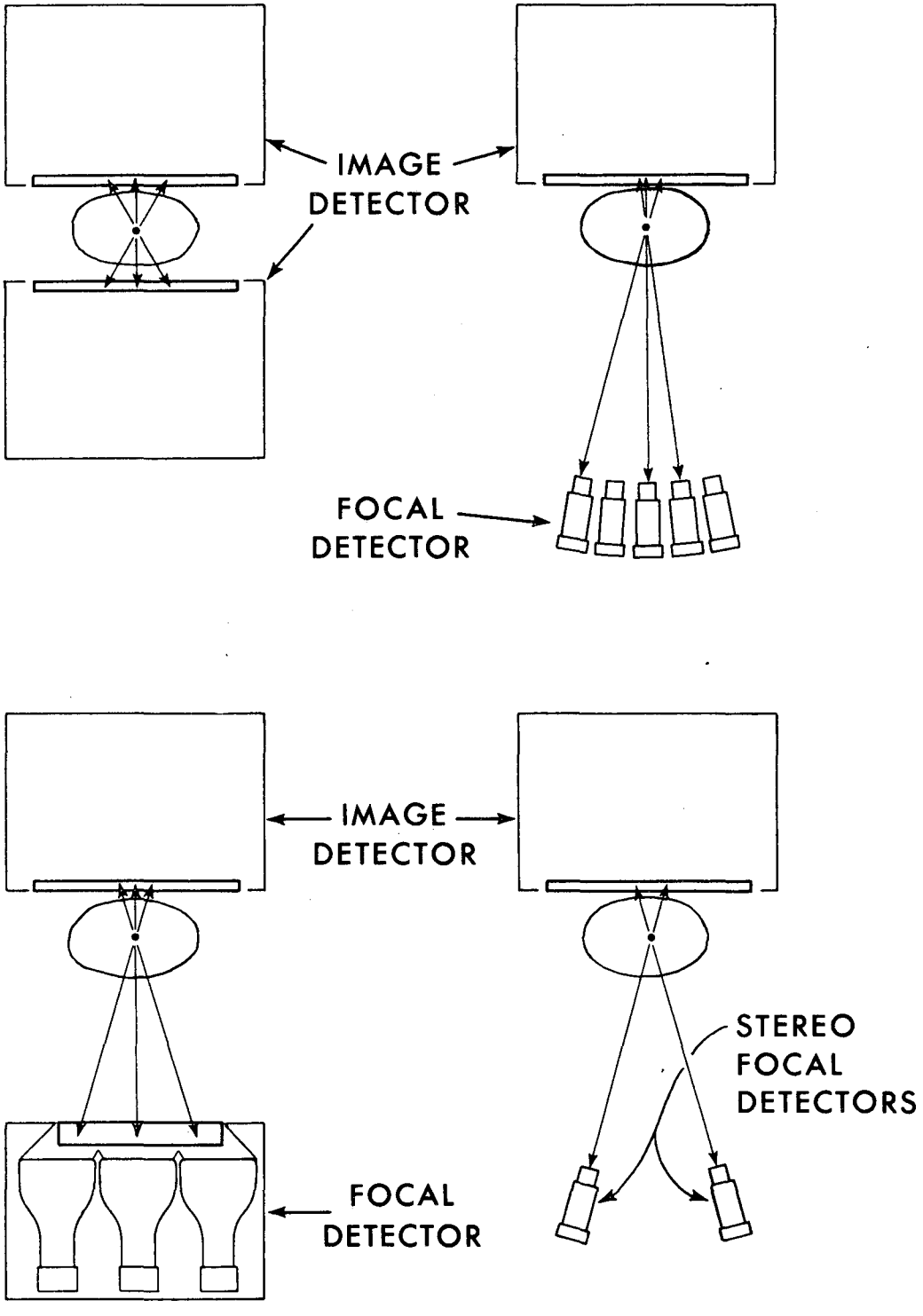

Fig. 22. (A, B, C) Various forms of focused positron camera. (D) Stereo positron camera.

momentarily when a coincidence occurs. The flashes are recorded by photographic time exposure, and an image of the positron distribution results. Other planes in the subject can be sharply resolved by taking weighted averages of the x and y pulses from the two detectors (6).

Disadvantages of the twin-detector method of imaging include relatively low sensitivity because both detectors use relatively thin scintillators. The overall sensitivity is proportional to the product of the photopeak detection efficiency of the two scintillators. Also, there is unnecessary complication due to the use of two high-resolution image detectors. This type of positron camera has been proposed (6,22) but never tried, because the following types have higher sensitivity.

Image Detector with Remote Multiunit Focal Detector. This type of positron camera uses a remote focal detector consisting of an array of scintillation counters with thick sodium iodide crystals, as shown in Fig. 22B. High sensitivity is obtained because of the high detection efficiency of the focal detector. At the same time, good resolution is maintained on any given plane in the subject by means of a dot-shifting technique described in detail in Section IVB.

Image Detector with Remote Imaging Focal Detector. The focal detector of this type of positron camera employs a large, thick solid sodium iodide crystal viewed by an array of 7 or 19 phototubes, as shown in Fig. 22C. The position of scintillations in the focal detector crystal is sensed by the same method as employed in the image detector. Slightly higher resolution can be obtained with this type of camera than with the multiunit focal detector because of the higher resolution of the imaging focal detector. Additional information is given in Section IVB.

Stereo Positron Camera. Stereo views of positron emitters can be obtained with one image detector and two remote focal detectors, as shown in Fig. 22D. The two focal detectors are located a short distance apart so that a 6- to 10-deg angle is formed between the subject and the two detectors. When a γ-ray pair is detected by the left detector, the flash on the image readout oscilloscope is shifted to the left half of the cathode-ray tube screen by means of a pulse generator triggered by the signal from the left detector. When a γ-ray pair is detected by the right focal detector, the flash is deflected to the right side of the screen. Thus two separate adjacent images constituting a stereo pair are formed, each associated with one of the focal detectors. They are recorded by photographic time exposure and later viewed in a stereo viewer. The 6- to 10-deg difference in viewpoint of the two detectors provides the necessary stereo separation. The focal detectors can be single counters as shown in Fig. 22D or they can be the more efficient position-sensing, types shown in Fig. 22B and C.

B. Operation of Focal Detector and Computing Circuits

A complete block diagram of a positron scintillation camera is shown in Fig. 7. At the top left is the image detector, and located 20 to 30 inches below is the focal detector, consisting of 19 scintillation counters in a close-packed hexagonal array, each with a 1-3/4-inch diameter by 2-inch-thick sodium iodide crystal. Pulse-height selectors adjusted to accept the 0.51-MeV photopeak are employed for both the image detector and focal detector.

The following description, though directed to the multiunit focal detector shown in Fig. 22B, also generally applies to the imaging focal detector shown in Fig. 22C. If a point source of positrons is located on a plane

below the image detector, as shown in Fig. 23, each of the 19 scintillation counters images the source as a separate disc at the image detector. The diameter d' of each disc is given by

$$d' = d\frac{a}{b},$$

where d is the diameter of each crystal in the focal detector, a is the distance from image detector to source, and b is the distance from the source to the focal detector. The distance c' between centers of the discs is given by

$$c' = c\frac{a}{b},$$

where c is the center-to-center distance between crystals in the array.

Although the 19 discs are spread over a wide area on the image detector crystal, they are superimposed on the image-readout oscilloscope by means of a dot-shifting technique. When a γ ray is detected by the center counter of the focal detector, the coincident scintillation in the image detector is shown on the image-readout oscilloscope without any shift from its normal location. However, when a γ ray is detected by any of the other 18 counters, a correction signal obtained from the focal detector shifts the position of the flash on the oscilloscope. The direction and magnitude of the correction signals are such that the 18 additional images of the point source are made to coincide with the image from the center counter. In other words, the point source is brought into focus. All other points lying on the same plane are also brought into focus by correction signals from the focal detector.

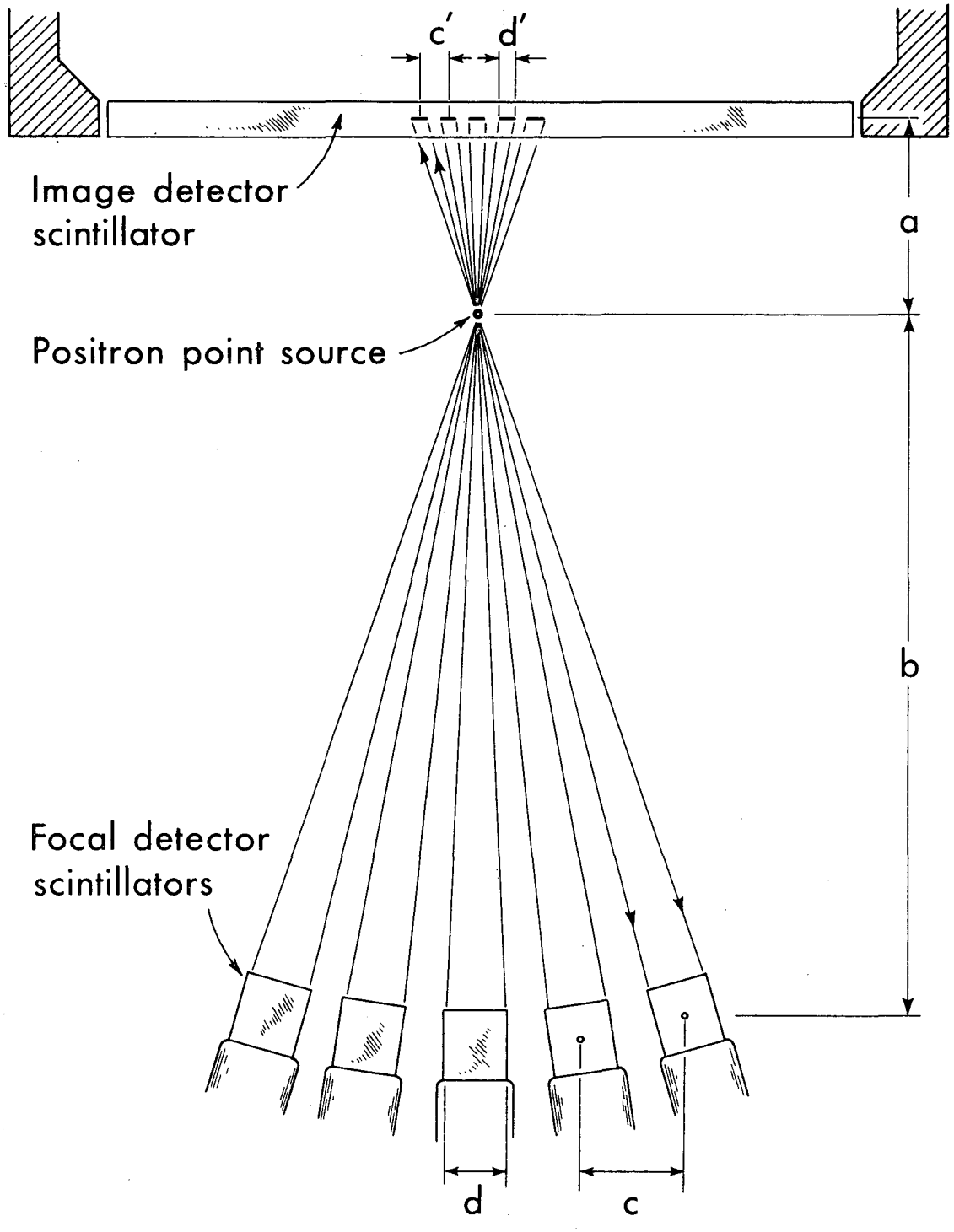

Fig. 23. Geometry of image formation in positron camera with multi-unit focal detector. The many images of the point source are superimposed on the image readout oscilloscope by means of a dot-shifting technique (8, 15)

The plane for which the correction signals are exact is called the "plane of best focus." This plane can be set to any desired level in the subject by means of the "focal plane selector," an attenuator shown in Fig. 7 that varies the strength of the correction signals. Since the electronic circuits are unable to sense the plane from which a γ-ray pair originates, the selection of the plane of best focus must be made by the operator. In a practical situation, the depth of an organ or tumor is often known, so the plane of best focus is set to that level. The resolution of nearby planes is improved by the same correction signals even though the correction is not exact. In other words, a certain depth of focus is obtained, just as with an optical camera.

An illustration of the depth of focus obtained is shown in Fig. 24. The subject was a rectangular array of 14 point sources of annihilation radiation with 1-inch center-to-center distance. The plane of best focus was set at 3 inches, and best resolution is obtained with the subject located 3 inches below the image detector. All most equally good resolution is obtained with the subject located at 2 or 4 inches, even though the "plane of best focus" remains at 3 inches. In a brain tumor phantom study, small "tumors" were found to be almost equally visible as long as they were within 2.5 inches of the plane of best focus (29).

C. Factors Affecting Resolution of Positron Cameras

Several factors affect the overall resolution of positron cameras.

Geometry of Image Formation. The geometric resolving distance R for positron cameras can be defined as the distance between two point sources located on the plane of best focus that are imaged as two tangent discs on the image detector. Then, referring to Fig. 23, it is apparent that

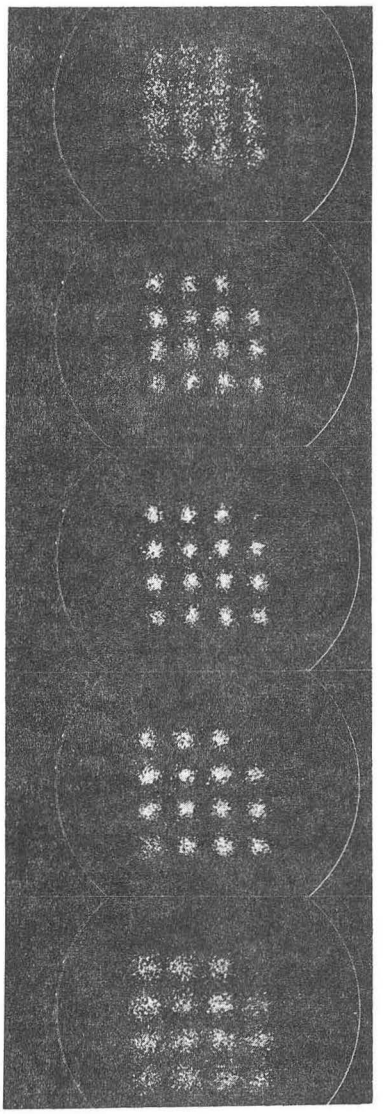

Fig. 24. Depth of focus of positron camera shown in Fig. 7. "Plane of best focus" was fixed at 3 inches and test source was located at 1, 2, 3, 4, and 5 inches.

$$R = \frac{ad}{b} .$$

To give an example of the geometric resolving distance obtained with the multiunit focal detector shown in Fig. 22B and Fig. 23, R is 0.27 inch or 7 mm when a = 4 inches, b = 22 inches, and the diameter d of the crystals in the focal detector is 1.75 inches.

When the imaging focal detector of Fig. 22C is used, the geometric resolution is better. Preliminary tests indicate that the inherent resolution of this focal detector is about 0.5 inch. Therefore the geometric resolving distance for point sources in the subject is about 0.08 inch or 2 mm. However, the inherent limitations in resolution of the present image detector prevent this high resolution from being realized in practice.

Inherent Resolution of the Image Detector. The inherent position resolution of the image detector has been discussed in Section IIC. At 0.51 MeV, the 19-phototube image detector is capable of resolving bars 5/32 inch wide and 5/32 inch apart in the central area of the scintillator. This corresponds to 0.16 inch or 4 mm resolution.

This resolution capability is maintained at count-rates up to about 10^7 scintillations per minute. When the integral count rate from the image detector exceeds this rate, resolution begins to decrease. The reason is that scintillations begin to overlap appreciably in time, and the flashes on the oscilloscope are displaced from their correct position. This is one of limitations of the scintillation camera that becomes apparent in the positron mode of operation. With no collimator between the subject and the image detector, the count rate can reach this value with 20 to 50 μC of positron

emitter located a few inches from the image detector. However, the sensitivity is such that with this amount of activity excellent pictures can be taken in a few minutes.

Range of positron particles in the subject. When a positron is emitted in tissue it travels a few millimeters before it comes to rest and combines with a negative electron. Since the γ-ray pair is produced at the end of the path, there is a loss of resolution. The loss is not peculiar to the positron camera, however, since all instruments which detect γ rays from positron emitters suffer from the same effect.

The maximum range of positrons in tissue is nearly the same as for β particles of the same energy and thus can be in the order of a centimeter or more. However, the average effective range is a small fraction of the maximum. First, each particle undergoes scattering along its path and the net distance traveled from the point of origin is but a fraction of the total distance traveled (20). Second, the average energy of positrons emitted in radioactive disintegrations is usually 0.4 to 0.5 times the maximum energy quoted in tables (42). Third, the average distance traveled perpendicular to the line of sight of the positron camera is a fraction of the net distance. The latter follows since the positrons are emitted isotropically and only the lateral travel causes a loss of resolution. As a result of all these factors the net average perpendicular distance traveled by positrons is about 1/4 of their maximum range. The resolution loss in soft tissue for 1-MeV positrons, for example, is about 2 mm.

Variation of annihilation γ-ray directions from 180 deg. When a positron is annihilated, the two γ rays travel away from their point of origin at almost, but not exactly, 180 deg. The variation from 180 deg is due to the fact that the velocity of the positrons is not quite zero when they combine

with an electron. They are slowed only to thermal velocity in tissue and the remaining momentum is transferred to the γ-ray pair. The resulting mean variation from antiparallelism is approximately 1/37 radian or 0.4 deg (26). The effect on resolution can be calculated by simple geometry. For example, the loss is only about 1/2 mm for a point source 4 inches from the image detector and 22 inches from the focal detector.

D. Sensitivity and Depth Response of Positron Cameras

The sensitivity of the positron camera shown in Fig. 7 can be calculated from

$$S = 4.44 \times 10^6 \; f_a \, \epsilon_I \, \epsilon_F \, f_t \, \frac{nd^2}{16\, b^2} ,$$

where S is the sensitivity in terms of the number of dots per minute produced on the picture per microcurie of positron emitter in the field of view of the camera, f_a is the abundance factor of the positron, ϵ_I and ϵ_F are the photopeak detection efficiencies of the image detector and focal detector, f_t is the total tissue absorption factor for both γ rays, d is the diameter of the focal detector crystals, n is the number of counters in the focal detector, and b is the distance from subject to focal detector.

When a subject is imaged completely within the boundaries of the image detector, the sensitivity is inversely proportional to the distance between subject and focal detector. Because this distance is usually large, the sensitivity is nearly constant when the subject is within a few inches of the image detector. This is the normal condition, since best resolution is then obtained.

The calculated sensitivity of a positron camera with an 11 1/2-inch-diameter by 1/2-inch-thick sodium iodide crystal and a focal detector

employing 19 separate counters with 1 3/4-inch-diameter by 2-inch-thick crystals is 1800 dots per minute per microcurie of 100% abundant positron emitter in air when the distance between image detector and focal detector is 22 inches. This agrees with that actually measured from calibrated sources.

The depth response in tissue of positron cameras is unique when compared with instruments that detect single γ rays. When the subject has a constant thickness, the response is largely independent of depth. This follows because both γ rays of a pair must be detected to produce a dot, and the total path length of the γ rays through tissue is constant. The total tissue absorption factor f_t is the same whether the γ-ray pair originates from the center of the subject or the top or bottom surface. It should be noted, however, that with subjects that vary in total thickness, the sensitivity is greater for the thinner parts of the subject because the total absorption of the two γ rays is less. This partly accounts for the brightness of the image at the edge of the patient's head in positron pictures taken of brain tumor patients.

The measured half-absorption thickness of 0.51-MeV γ rays in tissue is 3.6 inches. A subject 6 inches thick has an absorption factor of 0.31. Therefore, the net sensitivity of the above instrument is about 560 dots per minute per microcurie of 100% abundant positron emitter in subjects 6 inches thick.

E. Background of Positron Cameras

Stray Radiation. In the positron mode of operation, the background caused by cosmic rays and stray radioactivity is only a few counts per hour. This results from the stringent requirements for pulse height and time

coincidence in the two detectors. Therefore, long exposures of objects containing very little activity produce quite satisfactory pictures. However, background dots are produced by other causes, as discussed below.

Accidental Coincidences. At the high count rates often encountered in the image and focal detectors, the chance of accidental coincidences becomes appreciable. The result is dots at completely random locations on the pictures. The accidental rate N_A is given by

$$N_A = N_I N_F T,$$

where N_I and N_F are the count rates in counts per second for the image and focal detectors at the output of the pulse-height selectors and T is the coincidence gate width in seconds.

The present instrument operates satisfactorily at a gross count rate of 10^7 counts per minute in the image detector. The coincidence gate width is 0.25 microsecond, and the accidental coincidence rate at this gross count rate is about 200 per minute. The true coincidence rate from γ-ray pairs is about 24,000 per minute under the same conditions. The accidental rate is minimized by shielding both detectors from active parts of the subject outside the field of view of the camera, as shown in Fig. 7.

Coincidences Between Positron and γ Rays. Some radioisotopes emit one or more γ rays in coincidence with a positron. When these γ rays produce scintillations that pass the pulse-height selector, spurious dots result. A random background is produced, because there is no correlation between the directions of the γ-ray pair and the other γ rays. However, many positron emitters emit no coincident γ rays. Furthermore, all γ rays of less than 0.51 MeV are removed by pulse-height selection, and those with

enough energy to pass the pulse-height selector produce a relatively small increase in background compared with the other causes listed here.

Small-Angle Compton Scattering. The third and major cause of background dots, particularly in thick subjects, is small-angle scattering of the 0.51-MeV γ rays. This subject is discussed in general terms in Section IID2.

To illustrate the magnitude of the effect in thick positron-emitting subjects, the following case is considered. For a 6-inch-thick subject, as calculated from the Compton-scattering coefficients for soft tissue, about 77% of the γ-ray pairs will undergo Compton scattering before they escape from the subject. Less than 1% are stopped by photoelectric interactions, and 23% escape unscattered. At 0.51 MeV, the pulse-height resolution is typically 10% and the lower edge of the pulse-height selector window is usually set about 5% below the center of the photopeak. The upper edge of the window is set high enough to include the entire upper portion of the peak.

From the Compton scattering formula, a 0.51-MeV γ ray must be scattered 18.8 deg to lose 5% of its energy. From the Klein-Nishina distribution, 8.7% of Compton-scattered γ rays are deflected 18.8 deg or less. Therefore 6.7% of the original γ-ray pairs are scattered through small angles and are still capable of passing the pulse-height selector. The result is that 78% of the dots shown on the picture are correctly located, since they are produced from unscattered γ-ray pairs. The rest are mislocated by varying amounts depending upon the scattering angle and the distance from the point of scattering to the image detector. The scattered dots produce a diffuse halo around the active areas of a thick subject. The effect can be partially removed by background-subtraction techniques described in Section V.

F. Clinical Examples

Frontal and right lateral views of a patient's head with a brain tumor are shown in Fig. 25. The tracer compound was 700 μC of Ga^{68} EDTA, a positron emitter with a 68-minute half life obtained from a long-lived parent. In the lateral view, marker sources were placed at the corner of the patient's eye and the bottom of the ear lobe. In the frontal view markers were placed at the ear canals. A small tumor is visible in both views. The bright outline of the patient's head is caused by uptake in the skin and diploe, since EDTA goes to extracellular fluid space.

The distribution of erythropoetic bone marrow contained in a human subject with Osler's disease is shown in Fig. 26A. The patient was given 50 μC of Fe^{52}, a positron emitter with an 8-hour half life, and 8 hours later a series of 10-minute exposures was taken when only 25 μC of Fe^{52} were present in the patient's body. The distribution of bone marrow in a subject with mild secondary polycythemia is shown in Fig. 26B. The pictures are placed on a drawing of a skeleton for orientation. With this method the distribution of marrow in many subjects, including normals, has been determined. The clinical significance has been discussed in other publications (12,53,54).

The distribution of Fe^{18}, a 1.8-hour positron emitter, in a 4-year old girl with an undiagnosed hematologic disorder is shown in Fig. 27. She was given 120 μC, injected intravenously, and 5- to 6-minute exposures were taken starting 1 hour later. Less than the normal amount of fluorine concentrated in the epiphyses, the growing ends of the bones, in this subject.

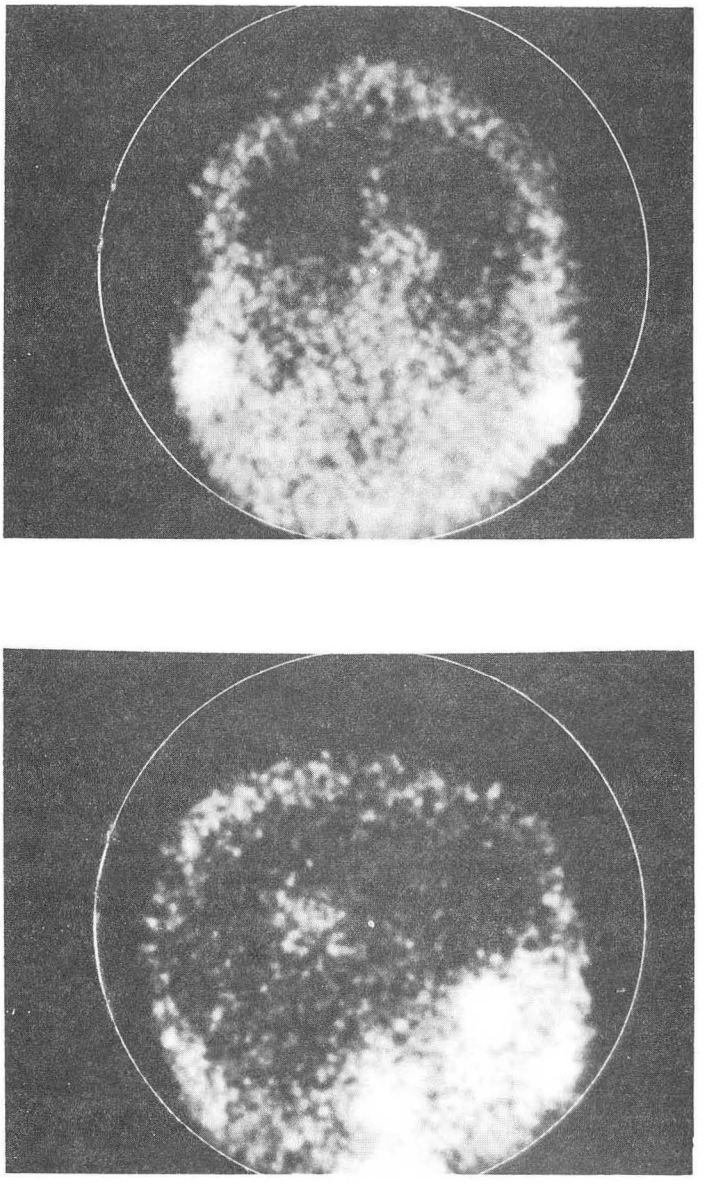

ZN-4775

Fig. 25. (A) Frontal and (B) lateral views showing brain tumor. Positron coincidence collimation was used, and Ga^{68}-EDTA was the tracer compound (7).

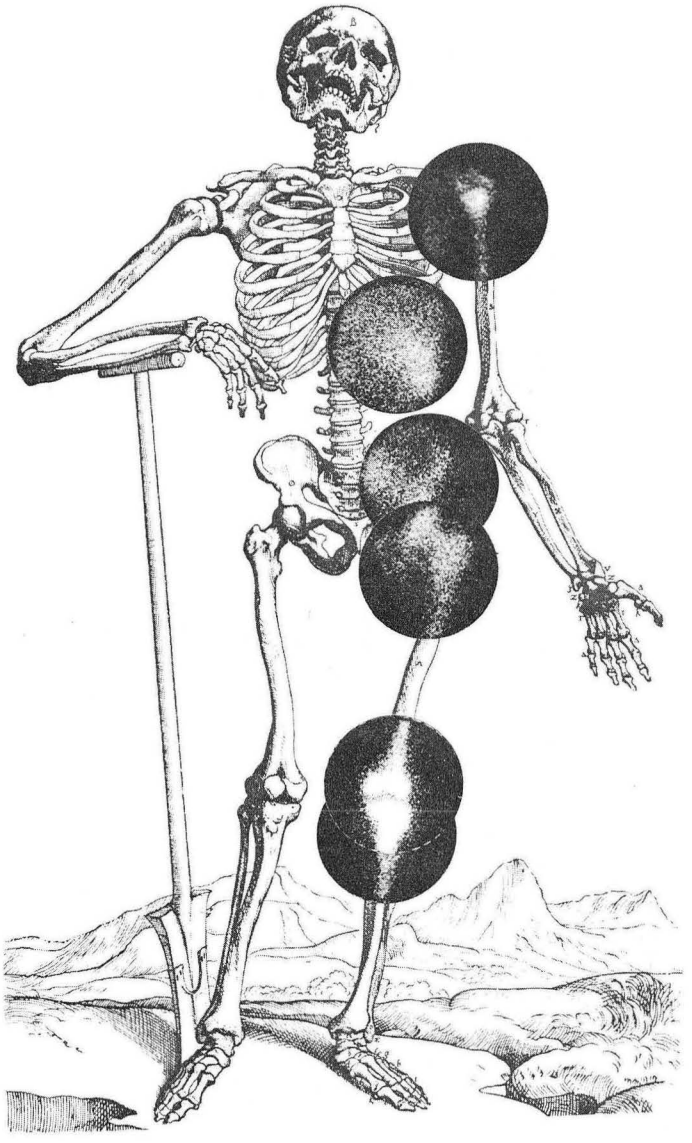

ZN-4779

Fig. 26. (A) Distribution of erythropoietic bone marrow in a man with chronic severe blood loss of many years' duration. Fifty μC of Fe^{52}, a positron emitter with an 8-hour half life, was administered, and about 8 hours later a series of 10-minute spot films was taken. Marrow is seen in the knee joint, a very unusual place for an adult. There is also an absence of marrow in the spine. (B) Virtually normal distribution of marrow is shown in this man with mild secondary polycythemia. About 100 μC of Fe^{52} was given and pictures were taken 16 hours later (12, 53, 54).

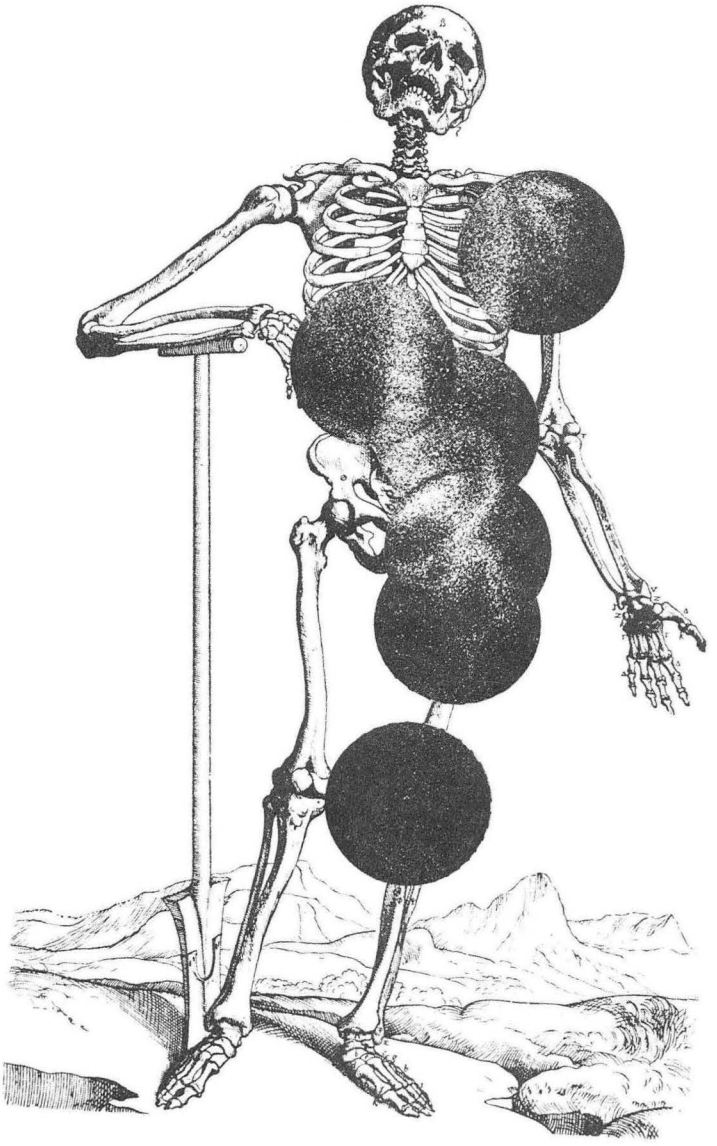

ZN-4780

Fig. 26b

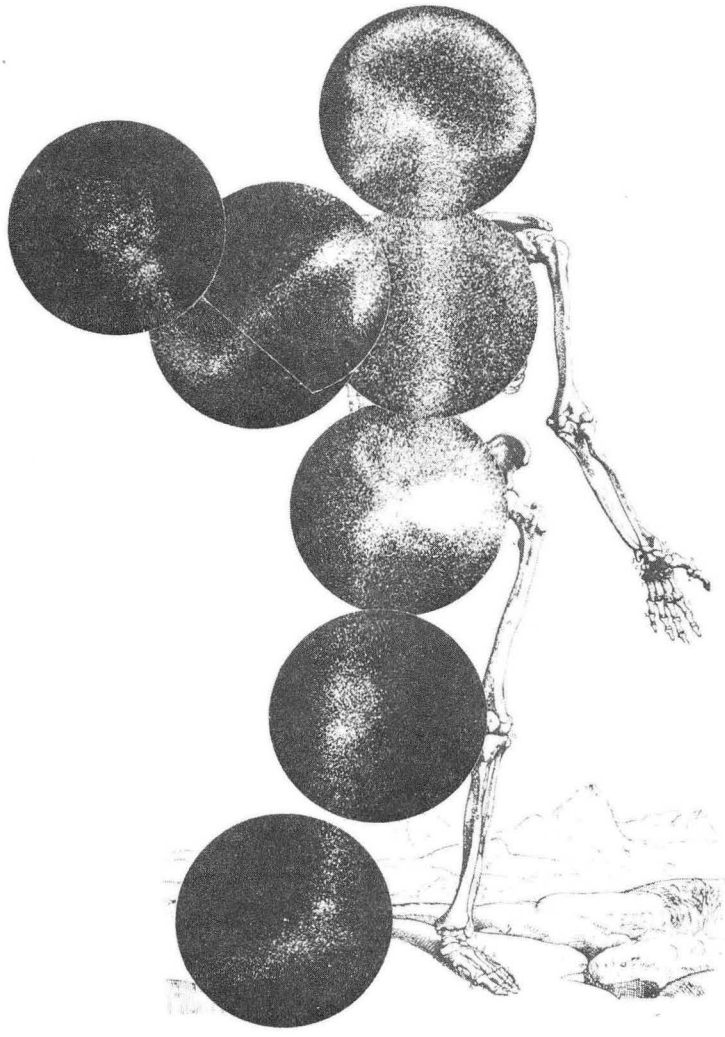

ZN-4777

Fig. 27. Distribution of F^{18} in a 4-year-old with hematologic disease. Pictures were taken 1 to 2 hours after injection, and exposure time was 4 to 6 minutes per field. Positron coincidence collimation was used with "plane of best focus" set at about 4 inches.

V. RECORDING METHODS

A. Image Recording and Viewing

Because most radioisotope cameras display individual γ rays as momentary point flashes of light on a readout screen, some method must be employed to record this information and form a time-integrated visual image. For maximum usefulness, the image should be available for viewing shortly after the exposure is finished or, even better, it should be visible during the exposure time as it builds up.

The recording method should avoid any permanent loss of data due to saturation effects or lower-level cutoff. Saturation causes loss of information in the more intense parts of the image. It can result when two flashes occur at the same point if the recording method does not permit the double event to be displayed as a more intense dot. Lower-level cutoff causes loss of information in the less intense parts of the image and can occur if the recording method requires two or more flashes at the same point before a visible response results. Though a lower-level cutoff is useful in minimizing the effects of background, it should normally be avoided in the initial recording, because loss of picture information can occur if it is set to the wrong level.

Another requirement is that the dots be recorded and displayed in such a way that the observer can best comprehend the image represented by them. Proper dot size is important. If the dots are small and there is much open space between them, it is difficult for the observer to perceive small differences in dot density. If the dots are too large, resolution is lost. A method of modifying dot size by means of diffusion is described

in Section VA2.

In displaying the pictures, a compromise should be made between contrast and gradation. Gradation refers to the number of gray tones visible due to increments in concentration of activity in the subject. Since amplifying contrast necessarily decreases gradation, contrast enhancement should be kept to the minimum necessary to show significant variations in the image. There is no point in amplifying contrast far beyond the point at which statistical variations become visible. When gradation is retained, images with large numbers of dots have depth and transparency. They display more significant information than high-contrast images. The latter look like silhouettes of an organ while the former show internal parts as well.

Finally, the observer should be free to judge the statistical validity of the image by being able to see the dot structure. Therefore, the dot structure of the pictures should not be permanently obscured by diffusion or defocusing. Otherwise, the observer can develop no sense of the statistical reliability of a picture.

1. Single-Lens or Multilens Oscilloscope Camera and Photographic Film

One method of recording images is to photograph the flashes appearing on the readout screen over a period of time with an optical camera and photographic film. If a single-lens oscilloscope camera and low-contrast film are used, proper exposure of the film is easily obtained. Contrast enhancement and background suppression can be obtained by viewing the picture on closed-circuit television (17,18). If medium- or high-contrast film is used for the initial recording, there is less exposure latitude, and proper exposure is more difficult to achieve when the dots are numerous enough to

overlap.

The exposure problem is easily solved by the multilens oscilloscope camera (8, 12) shown in Fig. 28. This optical camera has several small lenses with graded apertures mounted on a single lens board. Several small images of the cathode-ray tube screen are produced simultaneously on one sheet of film. Each lens allows a different amount of light to reach the film, and a range of over- to underexposure is achieved, with at least one satisfactory image assured. Subjects with considerable variation in amount of activity are rendered with no loss of information, because the most active parts of the subject receive proper exposure in one image and the less active parts in another. Furthermore, a wide range of exposure times can be used with no adjustment of the equipment. With long exposures, the slower lenses give satisfactory images, while with short exposures the faster lenses yield properly exposed images.

Of all the types of photographic film available, Polaroid self-developing film is most convenient, because the image can be seen a few seconds after the exposure is made. This film normally yields medium-contrast positive prints. In the density-versus-exposure characteristic, there is a threshold that must be exceeded before the film responds. The print remains black even though the film has been exposed to a certain amount of light, and then with very little more exposure it turns gray, and with still more exposure, white.

If the dots are numerous enough to pile up in parts of the image, the contrast characteristic of Polaroid film provides moderate contrast enhancement and a lower-level cutoff. Where the concentration of activity is below a certain level the image remains black, while parts of the subject above

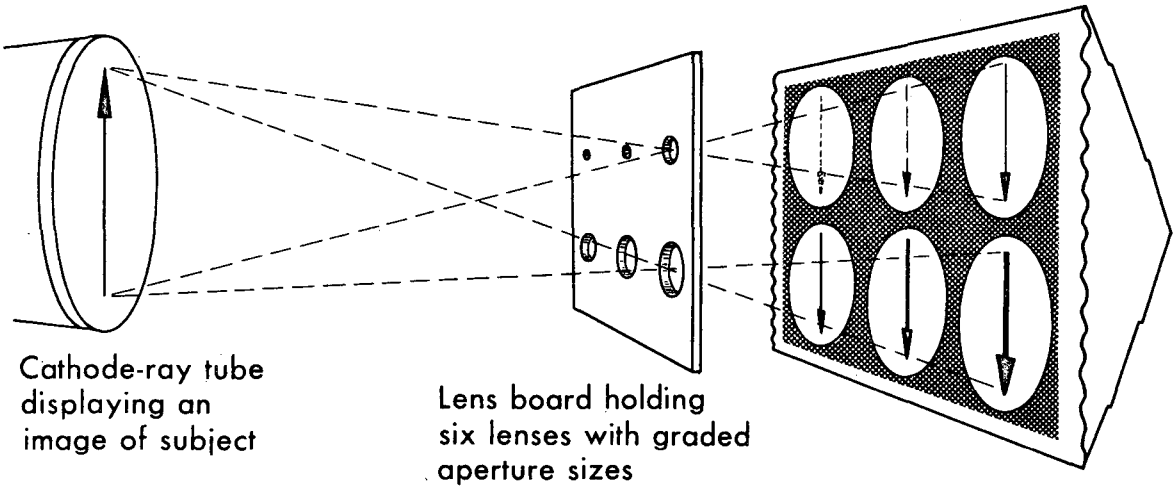

Fig. 28. Drawing of multilens oscilloscope camera, showing how images with graded intensity are formed.

the level are gray or white. The multilens camera thus gives a series of images with graded lower-level cutoff.

If the dots are not numerous enough to pile up, no contrast enhancement results from the use of moderate- or high-contrast film. When pictures are composed of only a small number of dots, the statistical variations are relatively great, and contrast enhancement has little or no value. The technique used at present is to record such pictures with sharply focused dots and view them through a diffusion filter as described in the following section.

A six-lens picture of a rat 1.5 hours after injection of F^{18} as the fluoride is shown in Fig. 29. Positron coincidence collimation was employed. All of the images were of course taken simultaneously. The first shows a diffuse outline of the rat and background dots. The third image shows a clearer outline of the rat and indicates that F^{18} is present in all the gross soft tissues. The fourth and fifth images begin to show the skeleton, where much of the F^{18} concentrates. The sixth picture shows only the parts of the skeleton having the highest concentration of F^{18}, the bladder, and one hydronephrotic kidney. Fluorine always appears in the bladder shortly after injection, since about 50% is cleared from the blood by the kidneys. However, the kidneys are not normally visualized. A histological examination was performed on the kidney, and distention of the kidney pelvis and blunting of the calices were found.

2. Gaussian Dot Diffusion

By viewing the pictures through a diffusion filter, different dot densities are transformed into different shades of gray (13,14). Little or no contrast enhancement is then necessary, because the human eye is quite

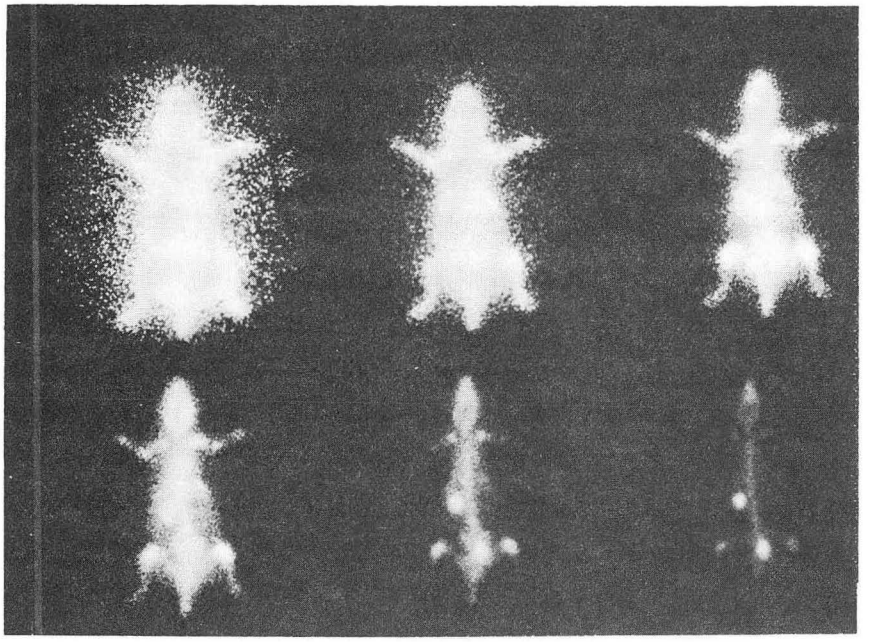

ZN-4781

Fig. 29. Example of picture taken with six-lens camera, showing distribution of F^{18} in a 200-gram rat in vivo. Twenty μC was administered intravenously, and 1.5 hours later a single 10-minute exposure was made, simultaneously producing six images with graded intensity.

sensitive to small differences in gray tones when the picture is adequately illuminated. Diffusion has the effect of suppressing background because isolated dots are defocused and blend into the background, where they become less noticeable. At the same time, parts of the picture with large numbers of dots per unit area are highligted, since the defocused dots add together to form a prominent bright area.

Diffusion of the pictures is particularly helpful for inexperienced observers. However, many experienced observers also find that it is easier to see variations in dot density through the filter. Familiar patterns in the subject become instantly recognizable, because the dot-density information is presented as a simple pattern of gray tones. It is no longer necessary to carefully examine each area of the picture to decide whether the area is more intense or not. It is obvious at a glance.

Examining the pictures through a minifying lens, or simply looking at them from a considerable distance, has somewhat the same effect as looking at them through the diffusion filter. The diffusion in the former cases is taking place in the eye of the observer. However, use of the filter has the advantage that the amount of diffusion can be easily varied, and the observer sees the picture in its normal size rather than as a tiny or distant image that is hard to examine carefully.

A satisfactory filter consists of a sheet of glass with a very finely pebbled surface, such as Tru-Site Picture Framing Glass (Dearborn Glass Co., Bedford Park, Illinois). With this filter the amount of diffusion obtained is directly proportional to the distance between the glass and the picture. The optimum amount is obtained by holding the glass at a distance determined by trial. If there is too little diffusion, the individual dots are still noticeable, and if there is too much, resolution is lost. With the

optimum amount of diffusion, the variations in dot density are changed to shades of gray with little or no resolution loss.

An example of the effect of diffusion is shown in Fig. 30. These pictures show the distribution of erythropoetic marrow in the shoulder area of a human subject. The tractor was 8.2-hour positron-emitting Fe^{52}, and coincidence collimation was used. In the sharply focused original, Fig. 30A, marrow is shown in the humerus, the clavicle, and the scapula. In the diffused copies, it is also easily seen in the ribs, the oblique lines at the lower left. It is easy to overlook the ribs in the original picture, although they can be seen is the observer looks for them. In the diffused pictures they are less likely to be missed.

A variation of the technique of viewing the sharply focused pictures through the diffusion filter is to record the picture initially with diffused dots. This can be done by placing the diffusion filter an inch or more in front of the cathode-ray tube. Alternatively it can be done by defocusing the cathode-ray beam with its focus control or by placing a defocusing lens in front of the scope camera. The use of the diffusion filter has the advantage that the light from each dot is spread into a nearly Gaussian pattern instead of a sharp-edged disc. The subjective effect of Gaussian diffusion is better than the other methods of defocusing. Furthermore, with the filter the diffusion is equal over the entire picture area, it is easy to vary the amount, and it does not vary if the f stop of the oscilloscope camera lens is changed, as it does if a defocusing lens is used.

Recording the pictures with diffused dots has the disadvantage that the diffusion cannot be reduced after the picture has been recorded. The method is satisfactory, however, in routine clinical situations for which the optimum

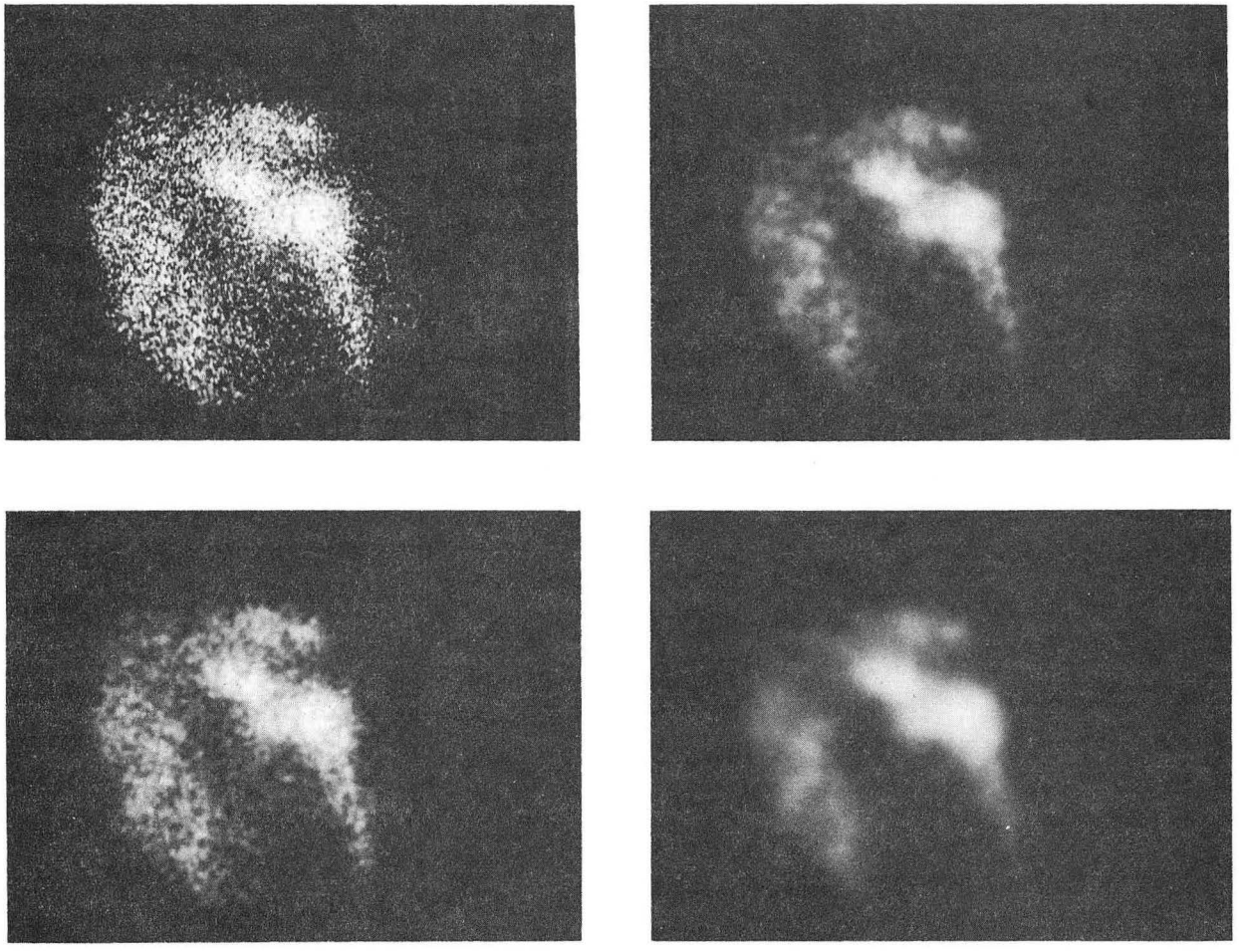

ZN-4226

Fig. 30. Effect of diffusion filter on picture originally recorded with sharply focused dots.

amount of diffusion is known. Alternatively, the pictures can be recorded with a small amount of diffusion and more can be added if necessary by observing them through the filter.

3. Memory-Type Cathode-Ray Tube

Mallard and Myers (43) reported constructing a γ-ray scintillation camera with a memory-type cathode-ray tube for readout and storage of the image. This is advantageous because the image is visible as it builds up. Thus, patients can be quickly positioned for the best possible view. Furthermore, the storage tube has a variable background suppression. After adjustment, the screen can be photographed to obtain a permanent record. Only significant pictures need be recorded.

The memory-type cathode-ray tube has a nonconducting storage mesh between a conventional electron gun and fluorescent screen. The electron gun deposits a charge on the storage screen at points corresponding to each dot in the image. This permits electrons from an electron "flood gun" to pass through and continuously illuminate a dot on the fluorescent screen. The image can be erased at any time by pressing a button that brings the potential of the storage mesh back to cutoff.

The requirements of a good storage tube are linear gray tone display, variable lower-level cutoff, adequate writing speed, and complete erasure of the previous image without residual effect on the following picture. Less ideal tubes can be used if their function is only to aid in aligning patients.

B. Motion Pictures

The movement of tracer compounds through organs can be shown either by taking motion pictures or by taking sequences of still pictures. Both show the dynamics of an organ, as well as its size and shape, and will

probably become increasingly valuable in medical diagnosis and research.

Two methods can be used for recording and displaying motion pictures. The first is to record the flashes from an image-readout oscilloscope with a motion picture camera. Usually the action is speeded up by exposing each frame for a few seconds or more and then projecting the developed film at the regular speed of 16 or 24 frames per second. A process that may take many minutes in the patient is compressed to a few seconds or viewing time.

A second method of displaying motion is to record the x- and y-position signals for each dot in the image on magnetic tape and play back the tape on a cathode-ray-tube monitor. By recording at slow tape speed and playing back at high speed, the action can be accelerated by factors of up to 100. The tape recording has the advantage that immediate playback is possible without the processing necessary for motion picture film. It also lends itself to obtaining numerical data, as described in Section VC.

One of the problems in viewing motion pictures of dynamic processes is to present the pictures to the observer so he can visualize the information contained in them. Each frame of a motion picture film is typically composed of a small number of dots. When these flash onto the screen for only a small fraction of a second, it is often difficult to visualize what they show.

One answer to the problem is the use of image-persistence techniques. The purpose of the latter is to make each dot remain on the screen long enough to make a suitable impression on the observer.

Image persistence can be obtained with closed-circuit television apparatus using a memory-type television camera tube called a Permachon (18). This special camera tube views the image-readout oscilloscope or a

projected motion picture, and the persistent image is viewed on a television monitor.

Image persistence can also be obtained by projecting an image from a motion picture projector onto a light-sensitive long-persistence phosphor and viewing the phosphorescent image. A third method is to reprint motion picture film by a "slip-frame" technique so that each frame on the original is printed on several frames of the copy. A fourth method is to view a magnetic-tape recording on a cathode-ray tube having a long-persistent phosphor.

C. Numerical Data Recording and Readout

Several methods can be used to obtain numerical count-rate data from specific areas of a picture.

Direct Electronic Methods. A relatively simple method is to divide the image into halves, quarters, etc., and electronically count the signals that produce dots within each area. For instance, to count flashes appearing on the right-hand half of the picture, a circuit that counts positive X signals but does not count negative X signals, is used. Another circuit sensitive only to negative X signals counts flashes appearing on the left-hand side of the picture. By sending the outputs of these two circuits to rate meters and a dual recorder, curves of the count rate versus time in the two halves of the image detector are obtained.

The above arrangement is used for kidney-function studies with I^{131} hippuran. The curves are comparable to conventional renograms.

Visual Dot Counting. This technique, used with the autofluoroscope by Bender and Blau (18), consists of recording flashes from an image-readout oscilloscope on motion picture film, then visually counting dots

within specified areas on each frame of the developed film. The number of counts per minute in the area is plotted as a function of time. This method is very flexible, since areas of any size or shape can be chosen, but it is laborius when large numbers of dots must be counted.

Magnetic Tape Recording with Numerical Readout. Numerical counts as a function of time can be obtained from a picture area of any size or shape by the following semi-automatic technique. First, the position and time of occurrence of all detected γ rays are recorded on magnetic tape. With the scintillation camera, this is done by recording all the X, Y, and Z pulses on a three-channel recorder. At the same time a picture of the organ under study is obtained from the readout oscilloscope with an optical camera.

Then by reference to the picture just obtained, a mask is made that blocks out all the picture except the area from which numerical counts are wanted. This mask is placed before the image-readout oscilloscope. Then the magnetic tape is played back and the flashes within the desired area are counted by a phototube. The counts are sent to a rate meter and recorded as a function of time on a chart recorder. Additional areas may be treated in the same fashion by making new masks and replaying the tape.

This method is very flexible because the position and time of all detected γ rays are recorded on the tape and numerical data from any area can be read out at any time in the future. It also offers the advantage that motion pictures or additional still pictures can be printed out by replaying the tape.

Magnetic Core Memory. Another method of obtaining numerical data from specific areas of a subject, consists of dividing the picture electronically into a rectangular mosaic of picture elements and storing the counts that occur within each element in a magnetic core memory. The memory systems used in multiparameter analyzers are suitable. These devices can

also display the stored data as intensity-modulated mosaic pictures on a cathode-ray tube with any desired amount of contrast amplification or background suppression. For instance, the data can be shown as an isocount image of the subject in which all picture elements with more than a certain number of stored counts are white and all with less are black. Also, the data can be shown as an isometric display of a three-dimensional plot, where the third dimension represents the number of counts stored in each channel.

To obtain numerical data from a specific picture area, the picture elements within that area are selected and the counts within those channels are totaled. If dynamic processes are being followed, the data in the memory are periodically transferred to another memory device, because the magnetic core memory alone does not record the time at which the counts in a particular channel were received. Then by the use of conventional computer techniques the numerical counts in the selected area are plotted as a function of time.

REFERENCES

1. Allen, H. C. Jr., and Risser, J. R., Simplified apparatus for brain tumor surveys, Nucleonics 13 No. 1, 28 (1955).
2. Anger, H. O., Use of a gamma-ray pinhole camera for in-vivo studies, Nature 170, 200 (1952).
3. Anger, H. O., Mortimer, R. K., and Tobias, C. A., Visualization of gamma-ray emitting isotopes in the human body, Proceedings of the International Conference on the Peaceful Uses of Atomic Energy, Vol. 14, 204 (United Nations, N. Y., 1956).
4. Anger, H. O., A new instrument for mapping gamma-ray emitters, Biology and Medicine Quarterly Report UCRL-3653, (Jan. 1957).
5. Anger, H. O., Scintillation camera, Rev. Sci. Instr. 29, 27 (1958).
6. Anger, H. O. and Rosenthal, D. J., Scintillation camera and positron camera, in Medical Radioisotope Scanning (International Atomic Energy Agency, Vienna, 1959), p. 59.
7. Anger, H. O. and Gottschalk, A., Localization of brain tumors with the positron scintillation camera, J. Nucl. Med. 4, 326 (1963).
8. Anger, H. O., Gamma-ray and positron scintillation camera, Nucleonics 21, No. 10, 56 (1963).
9. Anger, H. O., Scintillation camera with 11-inch crystal, in Donner Laboratory Semiannual Report UCRL-11184, Fall 1963, p. 69.
10. Anger, H. O. and Davis, D. H., Gamma-ray-detection efficiency and image resolution in sodium iodide, Rev. Sci. Instr. 35, 693 (1964). Also in Donner Laboratory Semiannual Report UCRL-11184, Fall 1963, p. 86.

11. Anger, H. O., Scintillation camera with multichannel collimators, J. Nucl. Med. 5, 515 (1964). Also in Lawrence Radiation Laboratory Report UCRL-11335, 1964.

12. Anger, H. O. and Van Dyke, D. C., Human bone marrow distribution shown in vivo by iron-52 and the positron scintillation camera, Science 144, 1587 (1964).

13. Anger, H. O., Scintillation camera image recording, Lawrence Radiation Laboratory Report UCRL-11336 (1964).

14. Anger, H. O., Van Dyke, D. C., Gottschalk, A., Yano, Y. and Schaer, L. R., The scintillation camera in diagnosis and research, Nucleonics 23, No. 1, 57 (1965).

15. Anger, H. O., Positron scintillation camera (in preparation).

16. Bender, M. A. and Blau, M., The clinical use of the autofluoroscope (Abstract), J. Nuclear Med. 3, 202, (1962).

17. Bender, M. A. and Blau, M., The autofluoroscope, in Progress in Medical Radioisotope Scanning, (Oak Ridge Institute of Nuclear Studies, Oak Ridge, Tenn., 1962), p. 151.

18. Bender, M. A. and Blau, M., The autofluoroscope, Nucleonics 21, No. 10, 52 (1963).

19. Bender, M. A., The digital autofluoroscope, IAEA Symposium, Athens (1964).

20. Berger, M. J., Monte Carlo calculation of the penetration and diffusion of fast charged particles, in Methods in Computational Physics, edited by B. Alder, S. Fernbach, and M. Rotenberg (Academic Press, Inc., New York, 1963), p. 135.

21. Brownell, G. L., Theory of radioisotope scanning, Int. J. App. Radiation and Isotopes 3, 181 (1958).

22. Brownell, G. L., Discussion on scintillation camera and positron camera, in Medical Radioisotope Scanning (International Atomic Energy Agency, Vienna, 1959), p. 79.

23. Brucer, M., Radioisotope scanning, ORINS-20 (1958).

24. Copeland, D. E. and Benjamin, E. W., Pinhole camera for gamma-ray sources, Nucleonics 5, No. 2, 44 (1949).

25. Davisson, C. M. and Evans, R. D., Gamma-ray absorption coefficients, Revs. Modern Phys. 24, 79 (1952).

26. De Benedetti, S. C. E., Owen, W. R., Konneker, C. and Primakoff, H., On the angular distribution of two-photon annihilation radiation, Phys. Rev. 82, 455 (1951).

27. Fucks, W. and Knipping, H. W., Eine gamma-retina,

Naturw. 42, 493 (1955).

28. Fucks, W., Knipping, H. W., Liese, E. and Schumacher, G., Isotopes in the clinic for heart diseases and cancer, Atomkerenergie 9, 271 (1964).

29. Gottschalk, A. and Anger, H. O., Sensitivity of the positron scintillation camera for detecting simulated brain tumors, Am. J. Roentgenol., Radium Therapy and Nucl. Med. 92, 174 (1964).
Also in Donner Laboratory Semiannual Report UCRL-11033, Spring 1963, p. 126.

30. Gottschalk, A. and Anger, H. O., Renal Scintiphatography with the gamma ray scintillation camera and Hg^{203} Neohydrin, Radiology (in press) (1965).

31. Gottschalk, A., McCormack, K. R., Adams, J. E. and Anger, H. O., A comparison of results of brain scanning using Ga^{68} EDTA----. Radiology 84, 502 (1965).

32. Gottschalk, A. and Anger, H. O., Use of the scintillation camera to reduce scanning time, J. Am. Med. Assn. (in press) (1965).

33. Gottschalk, A. and Anger, H. O., Progress in radioisotope scanning: Clinical application of scintillation cameras and short lived isotopes, in Progress in Atomic Medicine, Ed. by John H. Lawrence (Grune and Stratton, New York, 1965).

34. Grodstein, G. W., X-ray attenuation coefficients from 10 keV to 100 MeV, National Bureau of Standards Circular 583 (1957).

35. Gross, W., Schlesinger, E. B., and de Boves, S., A scintillation camera for kinetic studies of radioactive nuclides in the brain, IAEA Symposium, Athens (1964).

36. Harper, P. V., Becks, R., Charleston, D. and Lathrop, K. A., Optimization of a scanning method using Tc^{99m}, Nucleonics 22, No. 1 50 (1963).

37. Harris, C. C., Eason, H. O., Francis, J. E. Jr., and Bell, P. R., An oscilloscope monitor for scintillation spectrometers, J. Nuclear Med. 1, No. 4, 280 (1960).

38. Johansson, S. A. E. and Skanse, B., A photographic method of determining the distribution of radioactive material in vivo, Acta Radiologica 39, 317 (1953).

39. Kellershohn, C. and Pallerin, P., Scintillator grid localizes gamma emitters photographically, Nucleonics 13, No. 12, 34 (1955).

40. Kellershohn, C. and Pellerin, F., "Sur la possibilite d'utiliser un tube amplificateur d' image - - -.

Compt. Rend. Soc. Biol. 149, 533 (1955).

41. Kellershohn, C., Lansiart, A., Desgrez, A., Sur deux nouveaux types da detecteur pour camera a rayons X ou γ,

IAEA Symposium, Athens (1964).

42. Loevinger, R., Japha, E. M., and Brownell, G. L., Discrete radioisotope sources, in Radiation Dosimetry, edited by Gerald J. Hine and Gordon L. Brownell (Academic Press, Inc., New York, 1956), p. 693.

43. Mallard, J. R. and Myers, M. J., The performance of a gamma camera for the visualization of radioactive isotopes in vivo,

Phys. Med. Biol. 8, 165 (1963).

44. Mallard, J. R. and Myers, M. J., Clinical application of a gamma camera,

Phys. Med. Biol. 8, 183 (1963).

45. Mather, R. L., Gamma-ray collimator penetration and scattering effects, J. App. Phys. 28, 1200 (1957).

46. Mortimer, R. K., Anger, H. O., and Tobias, C. A., The gamma-ray pinhole camera with image amplifier, University of California Radiation Laboratory Report UCRL-2524 (1954). Also in Convention Record of the Institute of Radio Engineers, 1954 National Convention, Part 9, p. 2-5, pub. by The Institute of Radio Engineers, New York (1954).

47. Rabinowitz, J. L., Shockman, A. T., and Bogash, M., The in-vivo autoradiography of human prostate-a preliminary communication, J. Nucl. Med. 5, 72 (1964).

48. Ramm, W. J., Scintillation detectors, in Radiation Dosimetry, edited by Gerald J. Hine and Gordon L. Brownell (Academic Press, Inc., New York, 1956), p. 278.

49. Ross, D. A., Satterfield, M. M., Jordan, J. C., Harris, C. C., and Bell, P. R., Low energy gamma emitters in scanning and other clinical applications, Proceeding of the Sixth International Symposium on Radioactive Isotopes in Clinical Medicine and Research, Bad Gastein, Austria (1964).

50. Shirley, D. A., Applications of germanium gamma-ray detectors, Nucleonics 23, No. 3, 62 (1965).

51. Ter-Pogossian, M., Kastner, J. and Vest, T. B., Autofluorography of the thyroid gland by means of image amplification, Am. J. Roentgenol. Radium Therapy Nucl. Med. 81, 984 (1963).

52. Ter-Pogossian, M., Autofluorography with an x-ray image amplifier, IAEA Symposium, Athens (1964).

53. Van Dyke, D., Anger, H. O. and Pollycove, M., Effect of erythropoietic stimulation on marrow distribution in man, rabbit, and rat as shown with Fe^{59} and Fe^{52}, Blood 24, 356 (1964).

54. Van Dyke, D. C., and Anger, H. O., Patterns of marrow hypertrophy and atrophy in man, J. Nucl. Med. (in press) 1965.

55. Van Dyke, D., Anger, H. O., Yano, Y. and Bozzini, C., Bone blood flow shown with F^{18} and the positron camera, Am. J. Physiol. (in press) (1965).

56. Yano, Y. and Anger, H. O., Production and chemical processing of iron-52 for medical use, Int. J. App. Radiation and Isotopes (in press) 1965.

57. Yano, Y. and Anger, H. O., A gallium-68 positron cow for medical use, J. Nuclear Med. 5, 484 (1964).

58. Yasukochi, H., Study of the scintillation camera, Nippon Acta Radiologica 2, 246 (1964).

LEGAL NOTICE

TECHNICAL INFORMATION DIVISION
LAWRENCE RADIATION LABORATORY
UNIVERSITY OF CALIFORNIA
BERKELEY, CALIFORNIA 94720